



Article

Xylem Hydraulic Conductance Role in Kiwifruit Decline Syndrome Occurrence

Claudio Mandalà ¹, Stefano Monaco ¹, Luca Nari ², Chiara Morone ³, Francesco Palazzi ¹, Grazia Federica Bencresciuto ¹ and Laura Bardi ^{1,*}

- ¹ Research Centre for Engineering and Agro-Food Processing, CREA Council for Agricultural Research and Economics, 10135 Turin, Italy; claudio.mandala@crea.gov.it (C.M.); stefano.monaco@crea.gov.it (S.M.); francesco.palazzi@crea.gov.it (F.P.); graziafederica.bencresciuto@crea.gov.it (G.F.B.)
- ² AGRION, The Foundation for Research, Innovation and Technological Development of Piedmont Agriculture, 12030 Manta, Italy; lnari@agrion.it
- ³ Phytosanitary and Scientific-Technical Services Department, Agricultural and Food Directorate, Piedmont Region, 10144 Turin, Italy; chiara.morone@regione.piemonte.it
- * Correspondence: laura.bardi@crea.gov.it

Abstract: Kiwifruit decline syndrome (KiDS) has affected kiwifruit orchards for more than ten years in the Mediterranean area, severely compromising productivity and causing extensive uprooting. The affected plants go through an irreversible and fast wilting process. The problem has not been solved yet, and a single cause has not been identified. In this work, we carried out a survey on ten five-year-old healthy kiwifruit cv. Hayward plants cultivated in an area strongly affected by KiDS and characterised by a rising temperature and vapor pressure deficit (VPD). Five plants were located in a KiDS-affected orchard. Our goal was to assess the hydraulic conductance of asymptomatic plants in a KiDS-affected area where rising climate change stress is underway. Our hypothesis was that a rising temperature and VPD could impair xylem functionality, leading the plants to develop strategies of tolerance, such as vessel narrowing, or stress symptoms, such as cavitation or implosion, inducing a higher risk of KiDS onset. Hydraulic conductance was investigated using a physiological and morphological approach to detect trunk sap flow, trunk growth and daily diameter variations, leaf gas exchanges and temperature, stem water potential, and the root xylem vessel diameter and vulnerability to cavitation. A strong xylem vessel narrowing was observed in all plants, with the highest frequency in the 30–45 μm diameter class, which is an indicator of long-term adaptation to a rising VPD. In some plants, cavitation and implosion were also observed, which are indicative of a short-term stress response; this behaviour was detected in the plants in the KiDS-affected orchard, where a high leaf temperature ($>39\text{ }^{\circ}\text{C}$), low stomatal conductance ($<0.20\text{ mol H}_2\text{O m}^{-2}\text{ s}^{-1}$) and transpiration ($<3\text{ mmol H}_2\text{O m}^{-2}\text{ s}^{-1}$), low stem water potential ($<-1\text{ MPa}$), high vulnerability to cavitation ($3.7\text{ }\mu\text{m mm}^{-2}$), low trunk sap flow and high daily stem diameter variation confirmed the water stress status. The concurrence of climate stress and agronomic management in predisposing conditions favourable to KiDS onset are discussed, evidencing the role of soil preparation, propagation material and previous crop.

Keywords: kiwifruit decline syndrome; physiological disorder; hydraulic conductance; xylem vessels; cavitation; drought stress; climate change; agronomic management



Citation: Mandalà, C.; Monaco, S.; Nari, L.; Morone, C.; Palazzi, F.; Bencresciuto, G.F.; Bardi, L. Xylem Hydraulic Conductance Role in Kiwifruit Decline Syndrome Occurrence. *Horticulturae* **2024**, *10*, 392. <https://doi.org/10.3390/horticulturae10040392>

Academic Editors: Francisco Garcia-Sanchez and Lili Huang

Received: 13 February 2024

Revised: 23 March 2024

Accepted: 8 April 2024

Published: 11 April 2024



Copyright: © 2024 by the authors. Licensee MDPI, Basel, Switzerland. This article is an open access article distributed under the terms and conditions of the Creative Commons Attribution (CC BY) license (<https://creativecommons.org/licenses/by/4.0/>).

1. Introduction

The worldwide kiwifruit production in 2021 amounted to about 6,850,000 metric tons. The top kiwifruit-producing country in the world is China with approximately 2,380,787 metric tons per year; New Zealand is the second kiwifruit-producing country with about 628,496 metric tons per year, and Italy is the third with 416,060 metric tons produced annually [1].

Over the last decade, kiwifruit cultivation has been challenged by several threats. Serious damages to kiwifruit orchards arose from the bacterium *Pseudomonas syringae* pv. *actinidiae* [2], and recently, from the insect *Halyomorpha halys* [3]. Since 2012, a new syndrome has been reported in Italy, and in 2020, it affected 25% (6600 ha) of the Italian kiwifruit production area [4]; this value rose to about 36% (more than 9000 ha) in 2022, with regions such as Veneto and Piedmont severely compromised (>80% and 70% incidence, respectively) [5]. Since its appearance, the possible causes of this syndrome have been largely investigated, and several designations have been attributed to it—(i) KD = Kiwifruit Decline, (ii) KVD = Kiwifruit Vine Decline, (iii) KVDS = Kiwifruit Vine Decline Syndrome, (iv) KiDS = Kiwifruit Decline Syndrome, (v) KEDS = Kiwifruit Early Decline Syndrome and (vi) “*moria del kiwi*”—describing the same symptoms arising in the root system and the canopy. In the present work, we adopted the “KiDS” designation. In KiDS-affected plants, the roots show poor and superficial growth and widespread brown, soft-rotting areas, the cortical layers are hypertrophic and detached from the central cylinder, and fine feeder roots are absent; the canopy goes through an irreversible and fast wilting process, suddenly appearing in the middle of the vegetative season, with stunted fruit growth and drop. The root symptoms precede canopy wilting, and once affected, the plants usually die within 2 years [6–8].

Several factors have already been investigated in terms of the possible origin of this syndrome such as soil-borne pathogens, waterlogging, environmental conditions, agronomic and soil management, but none of the stress factors investigated so far can be considered the sole cause of KiDS onset [9–18]. Therefore, the occurrence of this syndrome is still unexplained, and it is generally recognised as the likely consequence of multiple concurring factors.

As symptoms start from the roots, most studies have focused on the soil, looking for possible biotic or abiotic stress factors. The study of soil microbioma has evidenced an association of KiDS-affected plants with a significant loss of microbial biodiversity and with the presence of opportunistic pathogens, such as oomycetes or saprophytic bacteria [6,13–15,17]. The improvement of soil biological fertility through the addition of organic matter or selected rhizospheric microbial consortia has been assessed, with scarce results, as the KiDS onset was not prevented [19,20]. Soil ridging and watering management aimed at avoiding water excess and flooding have also been tested, as kiwifruit roots are highly sensitive to hypoxic conditions, but also—these treatments were not sufficient to stop KiDS from spreading [16,18,20–25]. A recent statistical survey carried out using Multiple Correspondence Analysis (MCA) on 125 Italian kiwifruit orchards showed that seven factors were related to KiDS occurrence: the propagation material (from micropropagation), the age of the propagation material (one year), the presence of PSA (*Pseudomonas syringae* pv. *actinidiae*), the previous crop (tree crop), the soil cationic exchange capacity (CEC, low), soil salinity (low) and soil chalk (low) [26].

Recently, a possible role of climate change has been proposed, highlighting the influence of high air and soil temperatures and vapor pressure deficit (VPD) on kiwifruit plant physiology and anatomy [19,20,27–30]. Rising temperatures and a VPD following climate change are considered among the main causative agents of plant decline and reduced crop productivity [31,32]. Anisohydric plants, like kiwifruit, are particularly damaged by global warming, due to reduced stomatal sensitivity, which makes them more vulnerable to a rising VPD and a negative carbon balance induced by high temperatures, which prevents root growth; indeed, anisohydric plants do not even benefit from watering under drought stress [31]. Kiwifruit is also strongly vulnerable to hydraulic conductance failure due to very large xylem vessels, fleshy texture and a high evaporative demand [32,33]. According to the cohesion–tension theory of water transport, water molecules are pulled through the xylem under tension and due to hydrogen bonds among them, following the water potential gradient between leaves and roots. Then, the xylem must withstand both the mechanical stresses associated with negative pressure and the risk of air entering the hydraulic pathway. Therefore, transport failure can occur due to the collapse of the conduit walls (implosion)

or the rupture of the water column through air seeding (cavitation) [34–40]. Implosion may restrict hydraulic transport by reducing the conduit diameter and may also trigger cavitation [40]. The reduced hydraulic conductivity can determine a cascade of physiological responses such as the stomatal restriction of transpiration and photosynthesis [41,42] or leaf abscission [43].

Plants exposed to drought stress and to a high evaporative demand develop adaptation strategies to reduce the risk of cavitation and implosion, which can vary between different species and within the same species [31]. Frequently adopted strategies for long-term adaptation are decreasing the xylem vessel diameter, because large xylem vessels are more exposed to cavitation, and increasing the vessel wall thickness, because thinner walls are more exposed to implosion [31,37,44,45].

KiDS-affected plants' main symptom is wilting; thus, a possible involvement of hydraulic conductance failure can be assumed. Therefore, it can be hypothesised that climate could also play a role, concurring with other stress factors, in KiDS occurrence. In KiDS-affected plants, a decrease in the xylem vessel diameter has been reported, which can be considered a form of adaptation to drought stress and a rising VPD [20]. Climatic stress can also cause reduced photosynthetic activity, due to high temperatures and stomatal closure; this can result in a negative carbon balance, at the cost of xylogenesis and of vessels wall thickening, promoting the risk of implosion as well.

In this work, we carried out an in-field survey in a strongly KiDS-affected area in Northern Italy, where rising VPD and temperatures have been detected in recent decades [46], in order to explore the hydraulic conductance of cultivated kiwifruit plants. Ten healthy plants of *Actinidia chinensis* var. *deliciosa* (cv. Hayward) were chosen for the detection of physiological and morphological parameters related to water uptake and flow and the plant water status; the trunk sap flow rate, diameter growth and daily diameter variation and leaf temperature were monitored during two years. Physiological parameters were detected during the growing season. The leaf gas exchanges, stem water potential and root xylem vessel diameter, density and area were analysed, and the vulnerability to cavitation index was calculated. The soil temperature was also monitored, and weather data were collected from the nearest agrometeorological station. Five plants were chosen among the healthy plants in an orchard in which 40% of plants showed KiDS symptoms (O1), while another five plants were located in an orchard not affected by KiDS (O2). The two orchards were close, planted in the same year and similarly managed; they differed in terms of their planting conditions: soil preparation, previous crop and propagation material. Our goal was to assess and describe the hydraulic conductance of asymptomatic plants under productive conduction in a KiDS-affected area where rising temperatures and VPD were detected in recent decades. Our hypothesis was that the rising temperature and VPD impaired xylogenesis and xylem functionality, leading the plants to develop strategies of tolerance, such as vessel narrowing, or stress symptoms, such as cavitation or implosion, and that impaired hydraulic conductance could contribute to the exposure of plants to a higher risk of KiDS onset, mostly when subjected to other predisposing factors such as those previously identified [26]. As far as we know, the possible role of the hydraulic conductance in KiDS onset under a changing climate has not been explored so far. The newly acquired knowledge could contribute to focusing on possible effective strategies for agronomic management designed to prevent KiDS onset.

2. Materials and Methods

2.1. Trial Set Up

The study was carried out in two orchards located in the province of Cuneo in Piedmont (Northern Italy), where KiDS caused the uprooting of about 40% of kiwifruit orchards over the last 10 years. The locations of the site and of the investigated orchards are shown in Figure 1.

The orchards were very close but affected differently by KiDS; five plants were chosen among the healthy plants of the orchard in which 40% of plants showed KiDS symptoms

(O1), while the other five plants were located in an orchard not affected by KiDS (O2). The orchards were planted in the same year and similarly managed; they differed in their planting conditions: soil preparation, previous crop and propagation material (Table 1).

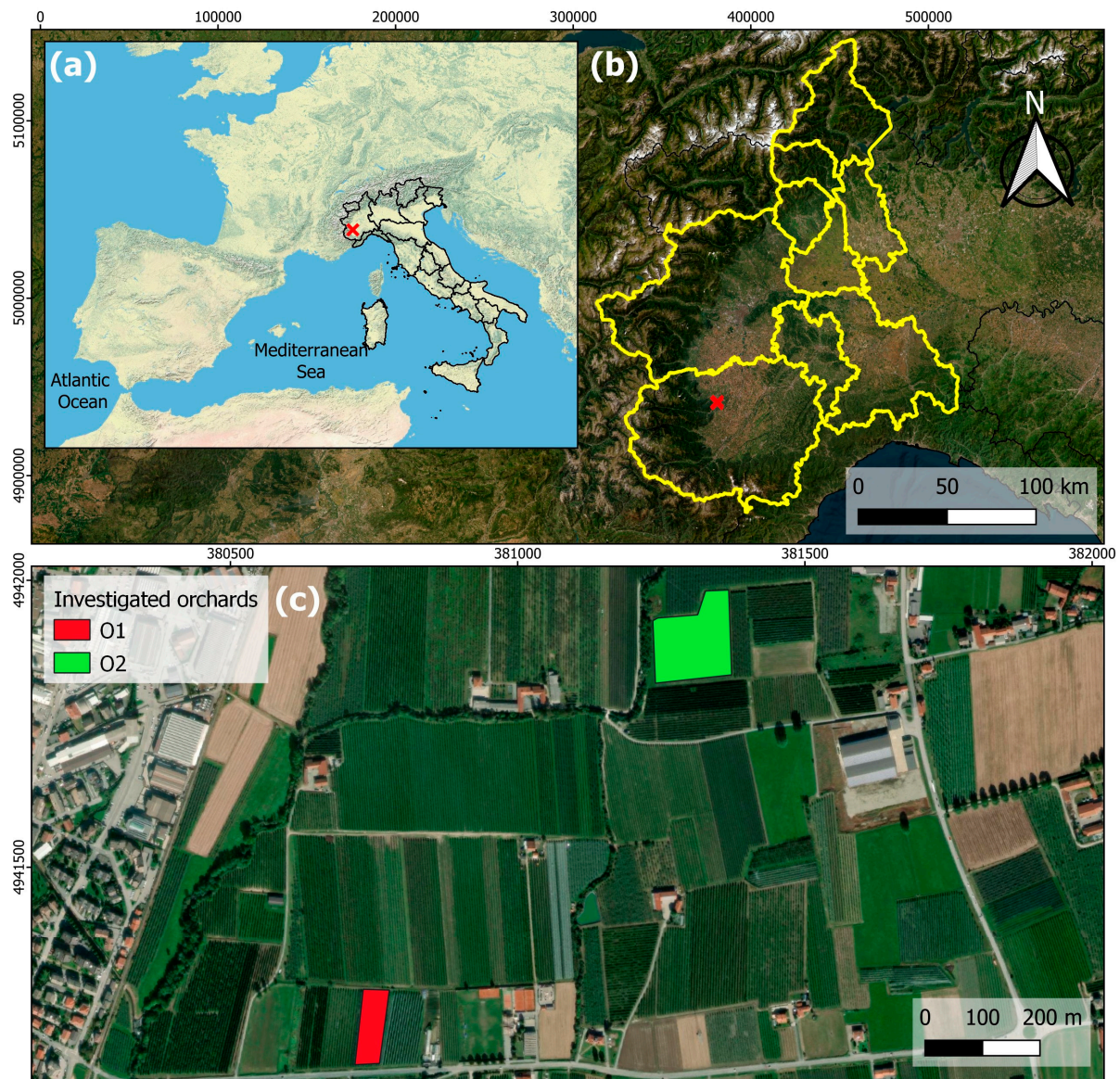


Figure 1. Location of the site (red cross in maps a and b) at (a) wide-area, (b) regional and (c) municipality scales. (c) shows the orchard presenting KiDS symptoms (O1) and orchard not affected by KiDS (O2), shown in red and green, respectively.

Table 1. Location and characteristics of the orchards.

	O1	O2
Coordinates	N 44.614417, E 7.497665	N 44.620674, E 7.503988
Farm management	Integrated Farming System	Integrated Farming System
Year of establishment	2017	2017
Cultivar	<i>Actinidia chinensis</i> var. <i>deliciosa</i> (Hayward)	<i>Actinidia chinensis</i> var. <i>deliciosa</i> (Hayward)
Training system	T-Bar (pergola)	T-Bar (pergola)
Planting distance	4.4 m × 3 m	5 m × 4 m
Plant number per ha	760	500

Table 1. Cont.

	O1	O2
Protection nets	Black anti-hail net	Black anti-hail net
Irrigation system	Drip system	Drip system
Propagation material	Micropropagation through meristem culture	Cuttings
Soil preparation	Flat soil	Soil ridging
Previous crop	Peach	Grass

The plants chosen were identified as follows: A, B, C, D and E in O1 and F, G, H, I and J in O2. B and J were male plants. Each plant was equipped with sensors for the monitoring of daily stem diameter variation and growth, trunk sap flow and leaf temperature; the monitoring lasted two years (2021 and 2022) and was stopped at the end of the second year due to the decision of the owner of O1 to uproot the row.

During the vegetative seasons, physiological determinations were carried out by detecting leaf gas exchanges and stem water potential. Anatomical analyses were carried out via light microscopy on roots sampled at the end of the vegetative season.

The soil temperature and water potential were monitored in both orchards, and weather data were collected from the nearest agrometeorological station. The data collected were analysed for the reference period corresponding to potentially greater climate stresses. The corresponding days of the year (DOYs) ranged from 154 (3 June) to 258 (15 September) for both years (2021 and 2022).

2.2. Field Site Description and Management

The location and main characteristics of the orchards are reported in Table 1.

The altitude and climatic zone were identical, and the agronomic management was very similar. According to the Köppen–Geiger classification [47,48], the area was characterised by a Cfa (i.e., warm temperate) climate, without a dry season and with hot summers. In both investigated orchards, the soils were classified as Dystric Fluventic Eutrodept, coarse-loamy, mixed, nonacid and mesic [49] or Fluvis Cambisol [50]. The physical and chemical soil characteristics of both orchards are reported in Table 2. The soil texture was loamy in both orchards, with a little lower clay and higher sand content in O2, which also showed higher values of organic carbon, CEC, a Ca/K ratio and assimilable iron, while assimilable phosphorus was lower.

Table 2. Physical and chemical soil characteristics of the orchards.

Physical Parameters	Unit	O1	O2
Clay	%	10.78	8.18
Silt	%	49.02	48.10
Sand	%	40.20	43.72
Chemical Parameters			
pH (water)	-	6.71	6.24
Total limestone	%	0.39	0.39
Organic matter	%	1.389	2.047
Organic carbon concentration	%	0.807	1.190
Total N content	%	0.1008	0.1551
C/N ratio	-	8.0	7.7
CEC—Cation exchange capacity	meq/100 g	11.8	15.1
Exchangeable calcium	ppm	1496	1709
Exchangeable calcium	meq/100 g	7.46	8.53
Exchangeable calcium as percentages of CEC	%	63.5	56.6
Exchangeable magnesium	ppm	159	157
Exchangeable magnesium	meq/100 g	1.31	1.29
Exchangeable magnesium as percentages of CEC	%	11.1	8.6
Exchangeable potassium	ppm	99	76
Exchangeable potassium	meq/100 g	0.254	0.195
Exchangeable potassium as percentages of CEC	%	0.022	0.013

Table 2. *Cont.*

Physical Parameters	Unit	O1	O2
Ca/Mg ratio	-	5.7	6.6
Ca/K ratio	-	29.4	43.7
Mg/K ratio	-	5.1	6.6
Base saturation	-	76.7	66.4
Assimilable phosphorus	ppm	43.7	17.2
Assimilable phosphorus pentoxide	ppm	100	39.3
Assimilable iron	ppm	86	150
Assimilable manganese	ppm	15.2	12.8
Assimilable zinc	ppm	3.6	2.6
Assimilable copper	ppm	5.7	4.7

Water management (Table 3) was carried out using a drip irrigation system, and the volumes required to restore soil depletion were determined based on soil moisture detected at two depths (20 cm and 40 cm) using soil moisture sensors (Watermark, Irrrometer Company Inc., Riverside, CA, USA). Overall, irrigation volumes in 2021 were higher in O1, particularly from August to October, while in 2022, in O2, they were more than double compared to those in O1.

Table 3. Irrigation volumes delivered in the monitored orchards during the reference period.

Year	Month	O1 [m ³ ha ⁻¹]	O2 [m ³ ha ⁻¹]
2021	May	0	0
	June	121	162.8
	July	344.4	344.1
	August	319.2	266.4
	September	218.4	140.6
	October	48.7	0
	Total	1052	914
2022	May	29.4	0
	June	222.6	555
	July	193.2	643.8
	August	193.2	414.4
	September	119.7	329.3
	October	0	0
	Total	758.1	1942.5

2.3. Environmental Measures

2.3.1. Weather Data

Weather data such as precipitation (mm), air temperature (°C), solar radiation (W m⁻²), relative humidity (%), wind speed (m s⁻¹) and vapour pressure deficit (VPD, kPa) were obtained from the nearest available weather station (METOS[®] station, Pessl Instruments GmbH, Weiz, Austria) (Coordinates N 44.658546, E 7.460144).

2.3.2. Soil Temperature

The soil temperature was monitored at two depths (20 cm and 40 cm) using temperature sensors, and the data were recorded using a datalogger (WATERMARK Monitor-900M) and downloaded periodically.

2.4. Physiological and Biometric Measures

2.4.1. Leaf Gas Exchanges

The measurements were carried out during 2021 (DOYs 195, 201, 209 and 215 at different times of the day: 09:30 a.m., 13:30 p.m. and 17:00 p.m.) and 2022 (DOY 143 in the morning between 09:30 and 11:30 a.m.) on five plants per orchard, and on three leaves (apical, young and fully developed) per plant.

Photosynthesis (A , $\mu\text{mol CO}_2 \text{ m}^{-2} \text{ s}^{-1}$), stomatal conductance (g_s , $\text{mol H}_2\text{O m}^{-2} \text{ s}^{-1}$) and transpiration (E , $\text{mmol H}_2\text{O m}^{-2} \text{ s}^{-1}$) were measured using an InfraRed Gas Analyser (IRGA, Portable Photosynthesis system Li-Cor, Ecosearch, Montone, Italy).

2.4.2. Stem Water Potential

The measurements were carried out during 2022 (DOY 143 between 13:00 and 14:30 p.m.) on five plants per orchard, and on two leaves per plant.

Leaves were covered with aluminium bags for 30 min to reach balance between leaf and stem water potentials and then picked from the middle of the shoot to measure the stem water potential (SWP, MPa) [51] using a pressure chamber (Ecosearch S.R.L., Montone, Italy) according to Scholander et al. [52].

2.4.3. Leaf Temperature

Leaf temperature was monitored using LT-1T sensors, and the data were logged using a data logging system SDI-12 Standard (version 1.3) (Edaphic Scientific, Melbourne, VIC, Australia) from June 2021 to September 2022 (DOYs 154–258); the sensors were placed on one leaf per plant in four plants per orchard.

2.4.4. Sap Flow

The trunk sap flow was monitored from June (DOY 154) 2021 to September (258) 2022 in five plants per orchard using a Heat Pulse Velocity Sensor (Implexx, Melbourne, VIC, Australia). The stainless steel needles had a diameter of 0.0013 m and length of 0.030 m, and a 0.006 m distance was between the heater and temperature needles. Negative temperature coefficient (NTC) thermistors, with an accuracy of ± 0.2 °C and a resolution of 0.001 °C, were in each temperature probe at 0.010 m and 0.020 m, respectively. The heater probe had a typical resistance of 38 Ω and dissipated approximately 4 W of power per 3 s heat pulse. The total energy applied per heat pulse was $\sim 400 \text{ J m}^{-1}$. The thermistors and heater element were controlled through a serial-to-digital interface (SDI-12, Implexx Sense, Melbourne, Australia) that measured temperature at a resolution of 0.2 and precisely controlled a 3 s heat pulse.

Data were logged at 30 min intervals using a data logging system (CR300 datalogger, Campbell scientific, Shepshed, Leicestershire, UK) and used to calculate the trunk cumulative sap flow (L) and the trunk daily sap flow rate (L/h^{-1}).

2.4.5. Dendrometric Measurements

Diameter dendrometers (DD-S2, Ecomatik, Munich, Germany) were placed in the trunk at a height of about 100 cm above ground on three plants per orchard. The sensor resolution was 0.2 μm and the accuracy was $\pm 0.1\%$. The data collected were used to calculate the trunk growth and the daily diameter variations.

2.5. Anatomical Analyses of Roots

2.5.1. Slice Preparation for Light Microscopy

At the end of the vegetative season in 2022, structural root samples (about 1 cm in diameter) were collected from each plant, rinsed under running water to remove soil residues and pre-treated in a 9:1 water–glycerol solution. Cross sections of 20 μm in thickness were obtained using a Leitz 1516 rotary microtome (Leica, Wetzlar, Germany) and bleached using a sodium hypochlorite 5% solution. After rinsing with water, slices were mounted on slides for microscopic analysis. The slides were observed using a Leica DM2000 LED light microscope (Leica, Wetzlar, Germany), and images were acquired using a digital camera (Leica DFC450C) and the Leica LASX 5.0.3.2480 software.

2.5.2. Image Analysis and Scripting and Xylem Vessel Measurements

ImageJ (open-source software) was used for image processing [53]. In detail, for this work, we used Fiji v2.14.0 [54], an updated version of the software enabling the ability to create codes using the programming language Python (v3.8), which allows the processing time to be accelerated [55].

The images acquired using the Leica LASX software were colour composites, i.e., each image consisted of different layers (or channels) that can be processed separately or merged into one RGB image. For this procedure, the composites were converted into binary 8-bit grayscale images, where every pixel corresponds to a digital number ranging from 0 (absolute black) to 255 (absolute white). The images were then processed using the built-in Threshold function. The aim of this step is to discriminate between white and grey-to-dark pixels. We observed that the most accurate thresholding results were obtained using the Triangle algorithm [56], which can be easily implemented and provides the best results when there is a dominant background peak. This method, also known as Minimum Error Thresholding, allows a threshold value to be selected that is able to minimise the difference between object and background pixels, while maximising the separability between the 2 classes of pixels. For this method, the threshold value was determined by normalising the height and dynamic range of the pixel intensity histogram of the image [57]. After the thresholding procedure was performed, the image was processed using the Analyze Particles function (also called ParticleAnalyzer, PA), returning information for each particle (i.e., each group of pixels that can be considered a separate item) within the image. Since white pixels could identify elements other than the xylem vessels (e.g., intracellular space, parenchymatic cells, etc.), thresholding values could be applied to minimise the PA's overestimation. Thresholding values regarding the minimum size of the elements and minimum circularity were specified. Circularity [58] is defined as follows:

$$\text{Circularity} = 4 \pi \cdot \frac{\text{Area}}{\text{Perimeter}^2}$$

with values ranging from 1 (i.e., a perfect circle) to 0 (i.e., an increasingly elongated polygon).

Three slices per plant were acquired and processed using ImageJ/Fiji v2.14.0. The PA was performed over a region of interest (ROI) of 1 mm². As a result, different parameters were obtained for every vessel observed within the ROI regarding area, perimeter and Feret's diameter.

Feret's diameter, which represents the longest distance between any two points along the boundary of an object [59,60], is considered a crucial metric for characterising the size and shape of plant structures (e.g., vessels) [61]. Its ability to capture the overall spatial dimensions of plant structures, enables variations in size and shape to be quantified and compared across different specimens and treatments within an experimental design. This metric proves particularly useful in assessing plant responses to environmental factors, growth conditions or genetic modifications, aiding in the understanding the physiological processes.

In each image, the xylem vessel density (vessels number mm⁻²), vessel area (µm mm⁻²) and vessel diameter (µm) were detected; the frequencies of distribution, classified by different diameter sizes, were also calculated.

2.5.3. Xylem Vessel Vulnerability to Cavitation Index (VI)

To assess and quantify the vulnerability to cavitation, the vulnerability index (VI) [62,63] was used, and it was calculated as follows:

$$VI = \frac{D}{V_D}$$

where D is the vessel diameter (µm), and V_D , the vessel density (vessel number mm⁻²).

2.6. Statistical Analysis

ANOVA and least significant difference (LSD) analyses were carried out by assuming a p -value threshold ≤ 0.05 . Data were processed using Excel (MS 16 Software) and PAST (v4.08) [64].

3. Results

3.1. Weather Data

Figure 2 shows the trend of the VPD and minimum, maximum and average air temperatures recorded during the reference period (from DOYs 154 to 258) in 2021 and 2022.

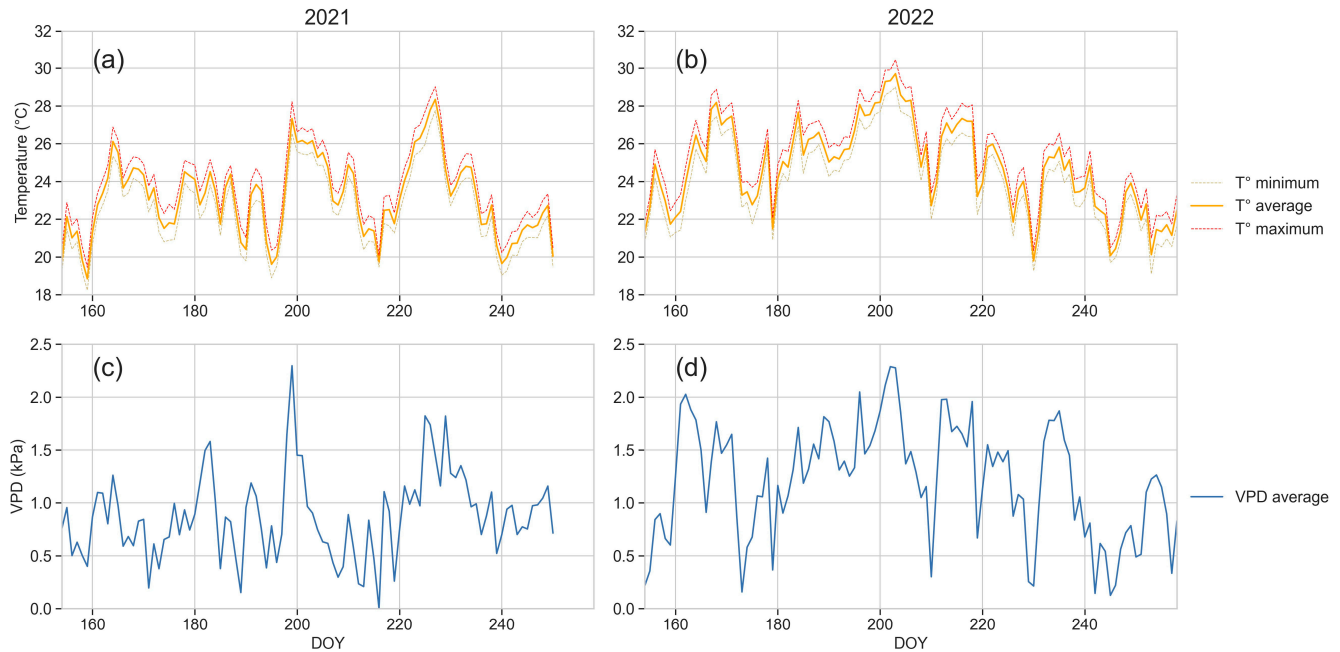


Figure 2. Trends of air temperature ($^{\circ}\text{C}$) (a,b) and VPD (kPa) (c,d) for the reference period in 2021 (a,c) and 2022 (b,d).

The weather data recorded during the two years are in line with the trends of growing temperatures and VPD observed during the last ten years within the study area [30]. As indicated in the annual regional reports from ARPA [65], 2022 was the warmest year for the whole historical climatic series (1958–2022) over the whole region.

The maximum daily temperatures reached very high values at DOY 227 (35.34°C) in 2021 and at DOY 206 (37.04°C) in 2022. The number of days with temperature values higher than 30°C were 41 and 75 in 2021 and 2022, respectively.

The VPD in 2021 was higher than 2 for 58 days, and higher than 3 for 8 days. In 2022 the number of days overpassing such thresholds increased, scoring VPD values higher than 2 for 77 days and higher than 3 for 31 days. The highest values detected were 3.97 in 2021 (DOY 199) and 3.78 in 2022 (DOY 203).

3.2. Soil Temperature

Figure 3 shows the trends for soil temperature at 0–20 cm (Figure 3a,b) and at 21–40 cm (Figure 3c,d) in O1 and O2 during the reference period (DOYs 154 to 258) in 2021 and 2022.

Soil temperature was always higher in O1 at both detected depths (20 and 40 cm) and remained higher than 20°C for long periods during summer. The soil temperature of O1 was higher in 2022 than in 2021 at both the superficial and deep layers.

3.3. Leaf Gas Exchanges

In Figure 4, the mean values of stomatal conductance (Figure 4a) and transpiration (Figure 4b) recorded during the growing season of five plants from O2 and O1 are reported. In Figure 5, the mean values of stomatal conductance and transpiration recorded during 2021 in different days and at different times of the day are reported.

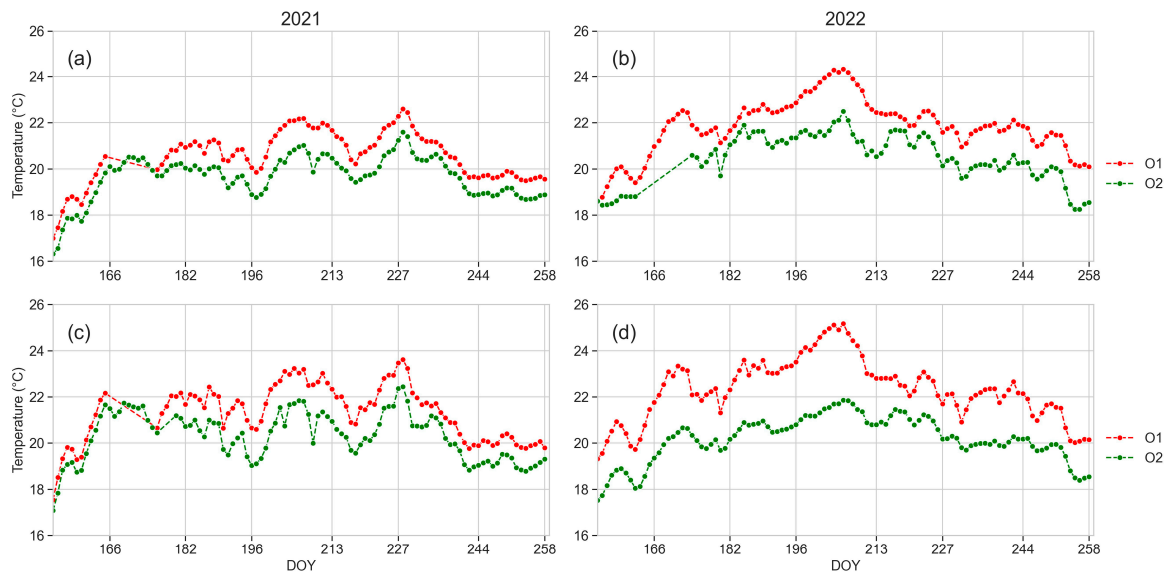


Figure 3. Trends for soil temperature at different depths: 0–20 (a,b) and 21–40 cm (c,d) in O1 and O2 during 2021 (a,c) and 2022 (b,d). Dotted lines indicate overridden missing data.

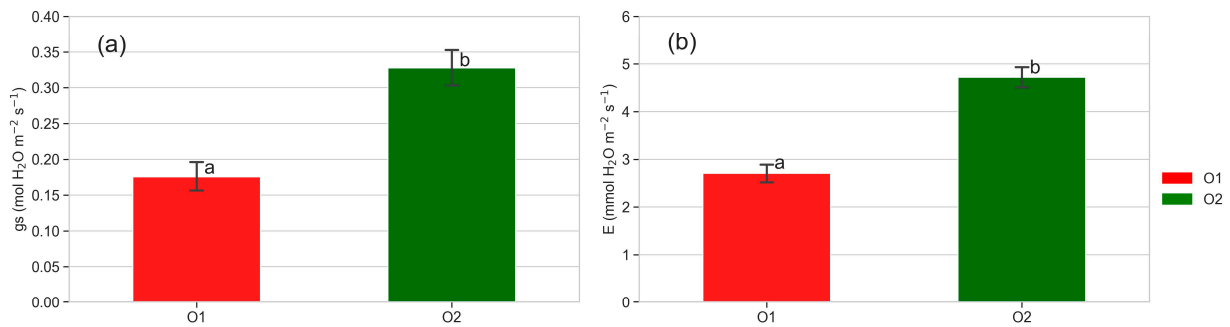


Figure 4. (a) Stomatal conductance (g_s , mol H₂O m⁻² s⁻¹) and (b) transpiration (E , mmol H₂O m⁻² s⁻¹) of plants from O2 and O1. Mean of 165 detections recorded on five plants per orchard throughout the growing season. Different letters show significant differences according to ANOVA and least significant difference (LSD) analyses at p -value threshold ≤ 0.05 .

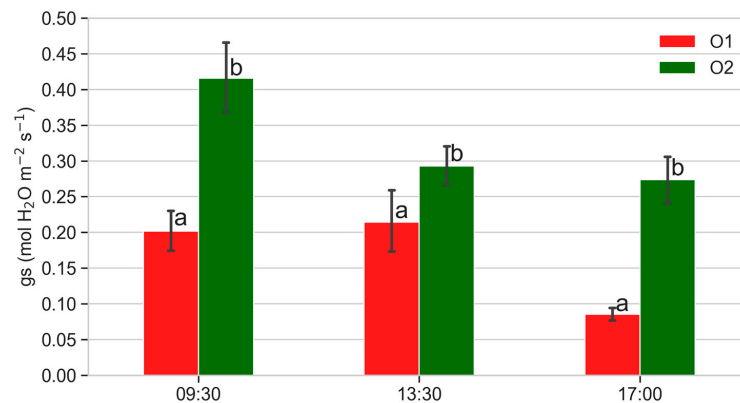


Figure 5. Stomatal conductance (g_s , mol H₂O m⁻² s⁻¹) of plants from O1 and O2 at different times of the day. Data are the mean of 50 measurements performed on five plants per orchard in 2021 on different days (DOYs 195, 201, 209, 215). Different letters show significant differences between data recorded at each time according to ANOVA and least significant difference (LSD) analyses at a p -value threshold ≤ 0.05 .

Stomatal conductance was always significantly lower in plants from O1 throughout the growing season (Figure 4a), especially in the morning and in the afternoon (Figure 5). Also, transpiration was lower in plants from O1 (Figure 4b). Figure 6 shows the relationship between photosynthesis and leaf stomatal conductance (Figure 6a) and the relationship between transpiration and leaf stomatal conductance (Figure 6b). Photosynthesis was related to stomatal conductance without differences between plants from O1 and O2, while transpiration was lower in plants from O1 when related to stomatal conductance (Figure 6b).

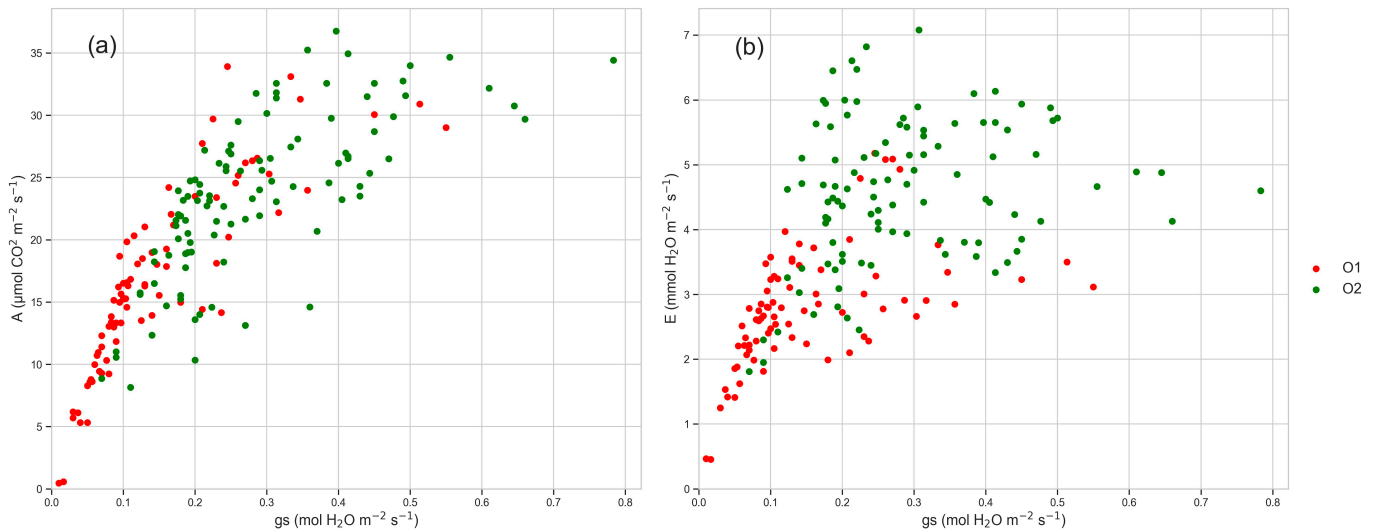


Figure 6. (a) Relationship between net CO₂ assimilation (A , $\mu\text{mol CO}_2 \text{ m}^{-2} \text{ s}^{-1}$) and leaf stomatal conductance (g_s , $\text{mol H}_2\text{O m}^{-2} \text{ s}^{-1}$) of plants from O1 and O2; (b) relationship between transpiration (E , $\text{mmol H}_2\text{O m}^{-2} \text{ s}^{-1}$) and leaf stomatal conductance (g_s , $\text{mol H}_2\text{O m}^{-2} \text{ s}^{-1}$) of plants from O1 and O2. Data were recorded throughout two years during growing season from June (DOY 152) to September (DOY 258).

3.4. Stem Water Potential (SWP)

Figure 7 shows the stem water potential recorded for plants from O1 and O2; the data shown are the mean values of the data recorded from five plants per orchard.

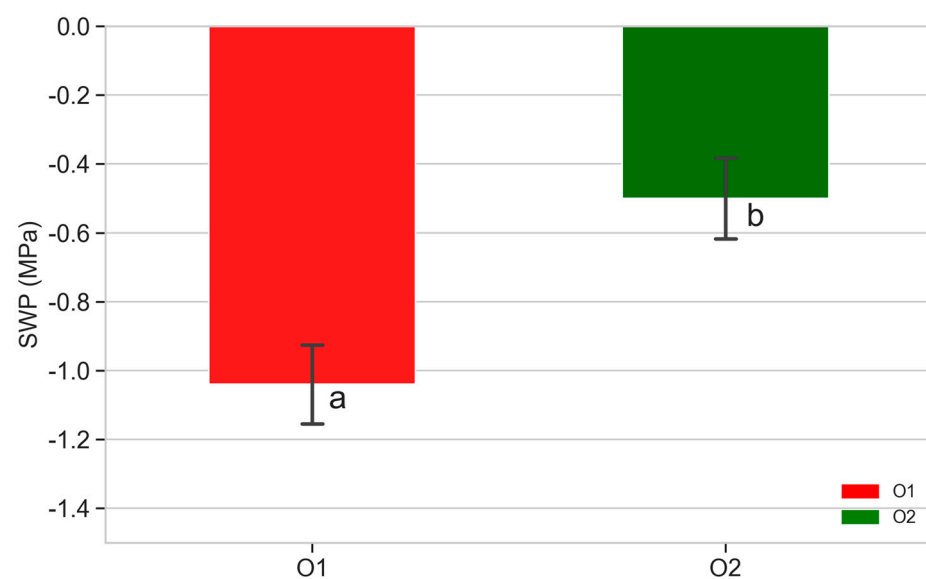


Figure 7. SWP of plants from O1 and O2. Mean values of data recorded from five plants per orchard in 2022 during summer (DOY 143). Different letters show significant differences according to ANOVA and least significant difference (LSD) analyses at p -value threshold ≤ 0.05 .

Significant differences were detected between plants from O1 and O2 for the SWP. The SWP ranged from -0.9 to -1.2 MPa in plants from O1, while in plants from O2, the values ranged from -0.4 to -0.7 MPa.

3.5. Leaf Temperature

Data of the daily maximum leaf temperature recorded in 2021 and 2022 from leaf temperature sensors are shown in Figure 8. The leaf temperature was always higher in plants from O1 than in O2, exceeding 30 °C during 82 days in 2021 (Figure 8a) and 89 days in 2022 (Figure 8b) in O1, and during 14 days and 25 days in 2021 and 2022, respectively in O2. Leaf temperatures exceeding 39 °C were detected only in O1, during 18 and 24 days in 2021 and 2022, respectively. Temperatures of 40 °C were recorded on DOYs 183 and 200 in 2021 in plants from O1, while the highest value was 34 °C on DOY 228 in plants from O2.

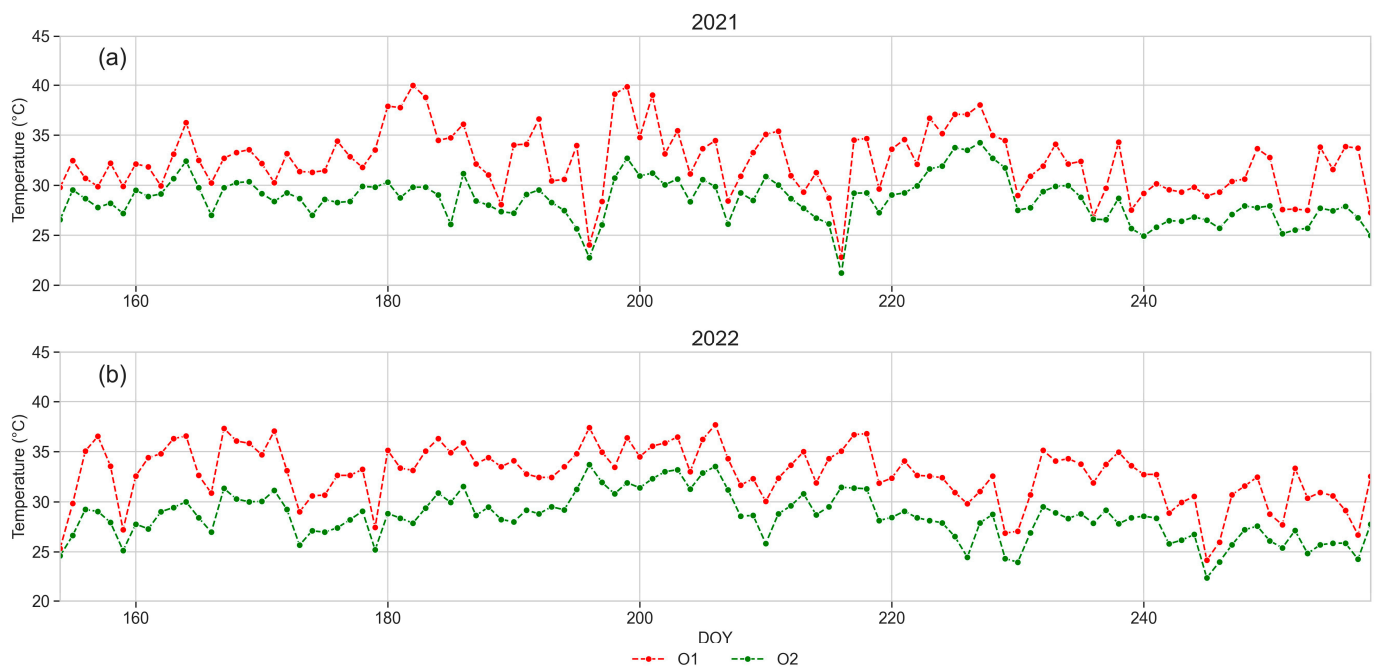


Figure 8. Daily maximum leaf temperature of plants from O1 and O2 monitored in 2021 and 2022 from June (DOY 152) to September (DOY 258). (a) year 2021, (b) year 2022. Daily mean values of data recorded from four plants in each orchard.

3.6. Sap Flow

In Figure 9, the values of sap flow recorded in 2021 and 2022 from plants from O1 and O2 are shown. The values of the sap flow rate, calculated as the mean of all data recorded from DOY 154 to DOY 258 are shown in Figure 9a, while the cumulative daily sap flow detected on DOY 258 is shown in Figure 9b.

Both the sap flow rate ($L h^{-1}$) and cumulative sap flow (L) were higher in plants from O2 compared to those from O1, with a strong difference in 2022. A discrete variability between the individual plants was observed: the final cumulative sap flow values at the end of the monitored period ranged from 320 L (plant J) to 695 L (plant I) in O2 and from 135 L (plant A) to 608 L (plant E) in O1 in 2021, and from 263 L (plant F) to 653 L (plant H) in O2 and from 90 L (plant A) to 204 L (plant E) in O1 in 2022.

The values of the daily stem sap flow rate recorded from June to September during the vegetative season of the two years (2021 and 2022) are shown in Figure 10. The daily stem sap flow rate showed diurnal variation characteristics, exhibiting a unimodal distribution every day. Plants from O1 showed a progressive decrease in the daily maximum flow rate starting from the second half of June 2021, becoming less than half in comparison to the plants from the O2 during summer and remaining low throughout the whole following year.

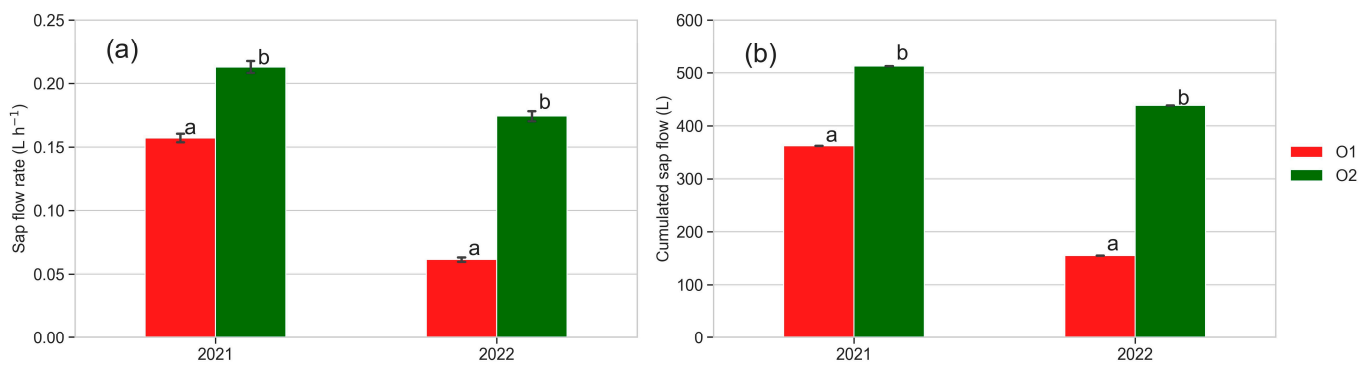


Figure 9. Sap flow rate ($L h^{-1}$) mean values of all data recorded from 3rd June (DOY 154) to 15th September (DOY 258) (a) and cumulative sap flow (L) detected at 15th September (DOY 258) (b); mean data of five plants per orchard. Different letters show significant differences according to ANOVA and least significant difference (LSD) analyses at p -value threshold ≤ 0.05 .

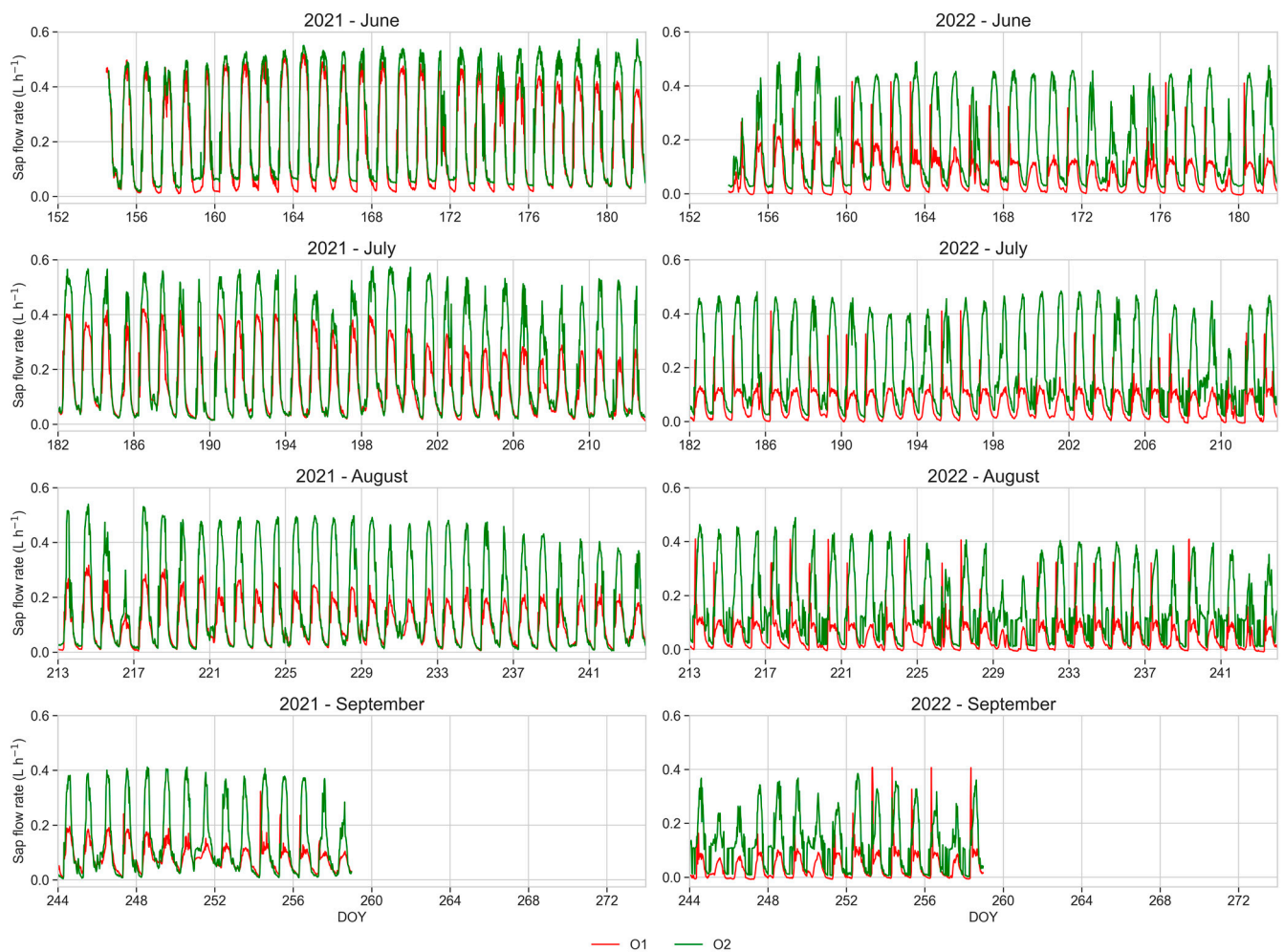


Figure 10. Daily sap flow rate ($L h^{-1}$) monitored during the vegetative season of the two years (2021 and 2022). Mean values of five monitored plants per orchard. Red line: O1; green line: O2.

The hourly frequency of the daily maximum sap flow rate shown in Figure 11 was different between O1 and O2: in O2, the peaks occurred between 1:00 and 2:00 p.m. in both years, while the most frequent occurrence in O1 was at 11:00 a.m. in 2021 and at 7:00 a.m. in 2022.

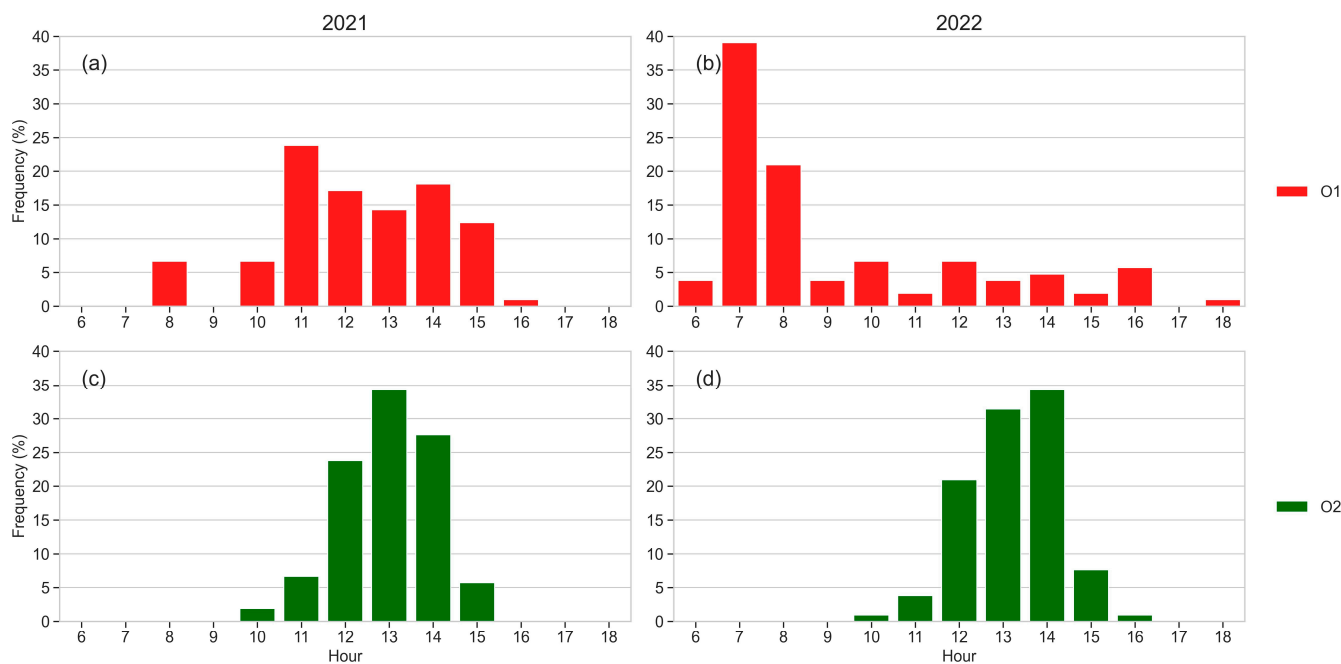


Figure 11. Hourly frequency of the daily maximum sap flow rate in 2021 (a,c) and 2022 (b,d). Mean values of five monitored plants per orchard. Green columns: O2 (a,b); red columns: O1 (c,d).

The plants with the highest cumulative sap flow were those in which the highest sap flow rate peak frequency dropped during the central hours of the day: in O1, the plants with peak values between 11:00 a.m. and 02:00 a.m. (C–E) showed higher cumulative sap flow values, while in the other plants, evidencing a lower cumulative sap flow (A, B), the sap flow rate dropped during the central hours of the day.

3.7. Dendrometric Measurements

Trunk diameter growth and daily cycles of diameter fluctuations monitored during vegetative season (from DOY 154 to 258) of the two years 2021 and 2022 are reported in Figure 12.

In both years, a regular trunk growth was detected within O2 from June (DOY 152) until DOY 244 (2021) and DOY 240 (2022), followed by a slightly slowing growth rate. In 2021, trunk growth started regularly within O1 in June (DOY 152), but it showed an early slowing from DOY 175 until mid-July (DOY 196), when the growth stopped; in 2022, the growth was almost nil.

The daily stem diameter variations, resulting from the cycles of shrinkage and swelling during the day as a consequence of the water status of the tree [66,67], were much larger in plants from O1, particularly during the second year.

The superposed daily dynamics of the sap flow rate and stem diameter are reported for some sample days in Figure 13. It can be observed that these dynamics correspond to the model proposed by Herzog et al. [68] for plants from O2 (Figure 13b), while the maximum sap flow rate detected early in the morning in plants from O1 corresponds exactly to the maximum stem diameter (Figure 13a).

3.8. Root Xylem Vessel Diameters

The distributions of the vessel diameter sizes of each plant examined and of the mean value of five plants per orchard are reported in Figure 14. The plants from O2 were characterised by a higher frequency of vessels within a diameter ranging from 31 to 45 μm (mean value 35%), with a maximum >60% in plant J and the exception of plant F, of which its maximum was in the 46–60 μm class. The diameter of the vessels was never higher than 135 μm within the O2 plants, except for plant G, while plants from O1 showed a broader distribution toward wider diameters, reaching 210 μm . Also, the frequency mean value of

plants from O1 was highest in the 31 to 45 μm class, but it was lower (<25%), and in plant B, the maximum was in the 121–135 μm class.

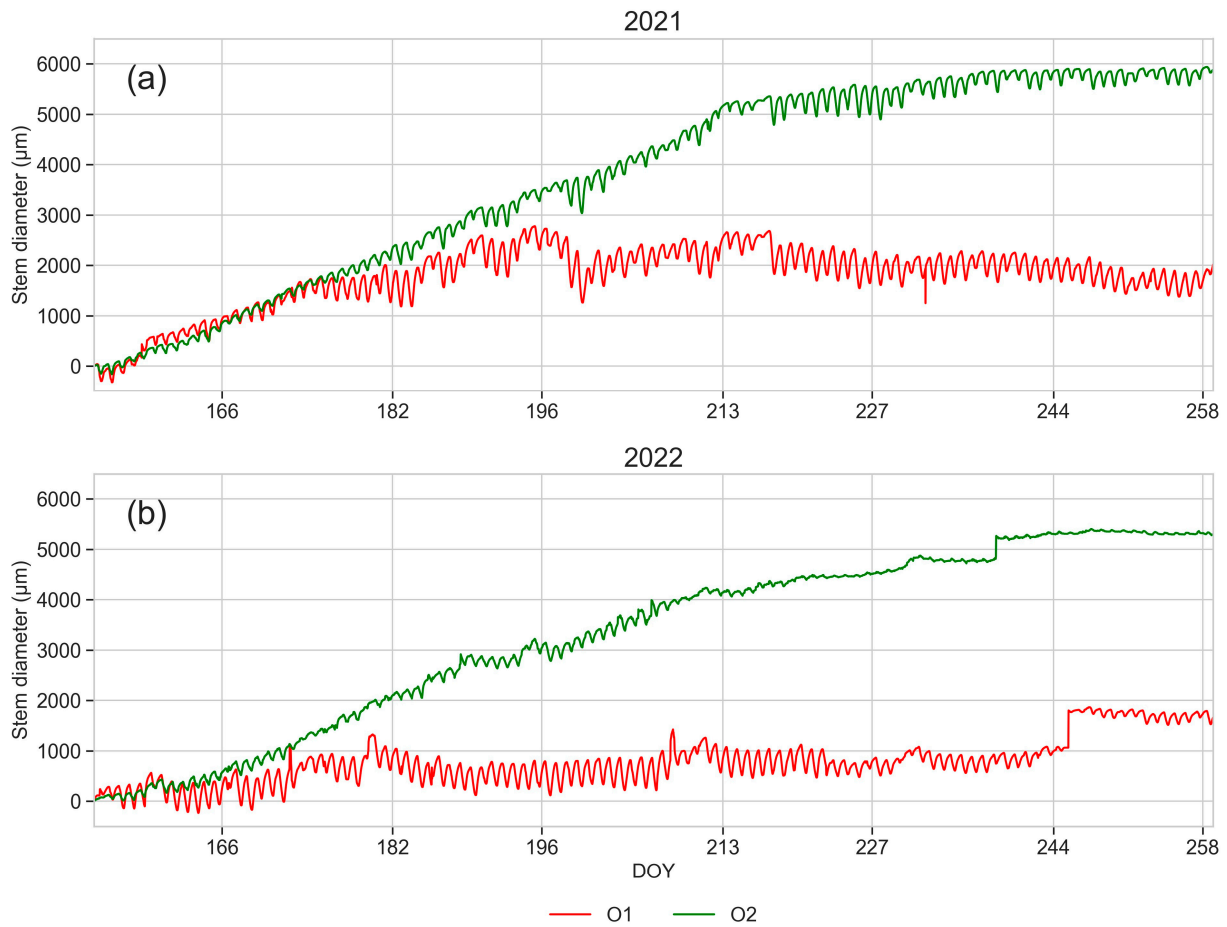


Figure 12. Stem diameter dynamics monitored using dendrometric measurements from 3rd June (DOY 154) to 15th September (DOY 258): 2021 (a) and 2022 (b). Mean values of five monitored plants per orchard. Green line: O2; red line: O1.

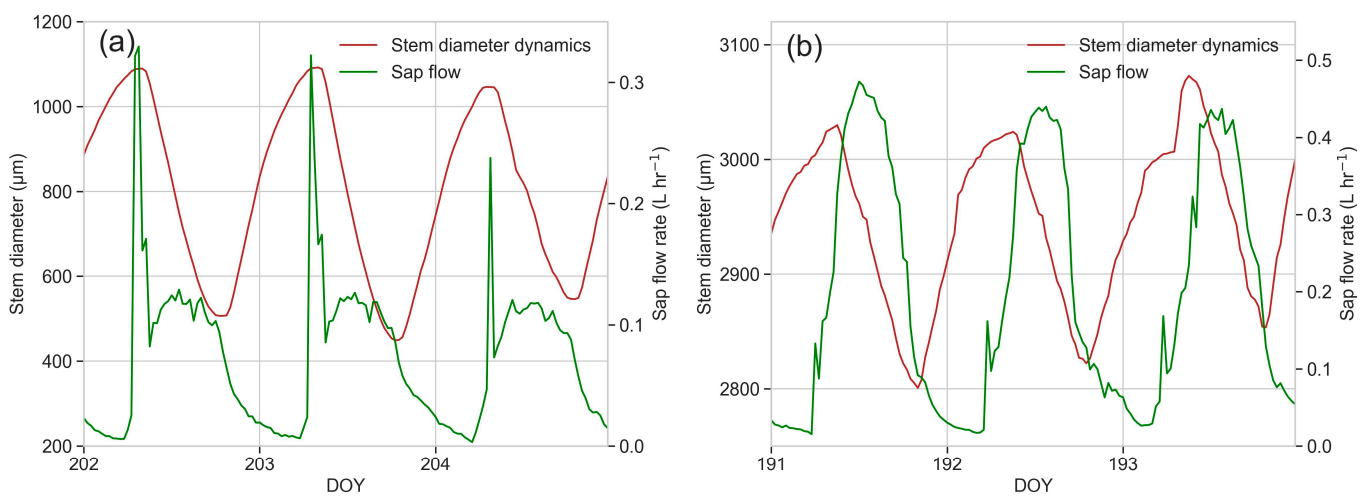


Figure 13. Daily dynamics of stem diameter (primary Y-axis, red line) and sap flow rate (secondary Y-axis, green line) in plants from (a) O1 and (b) O2.

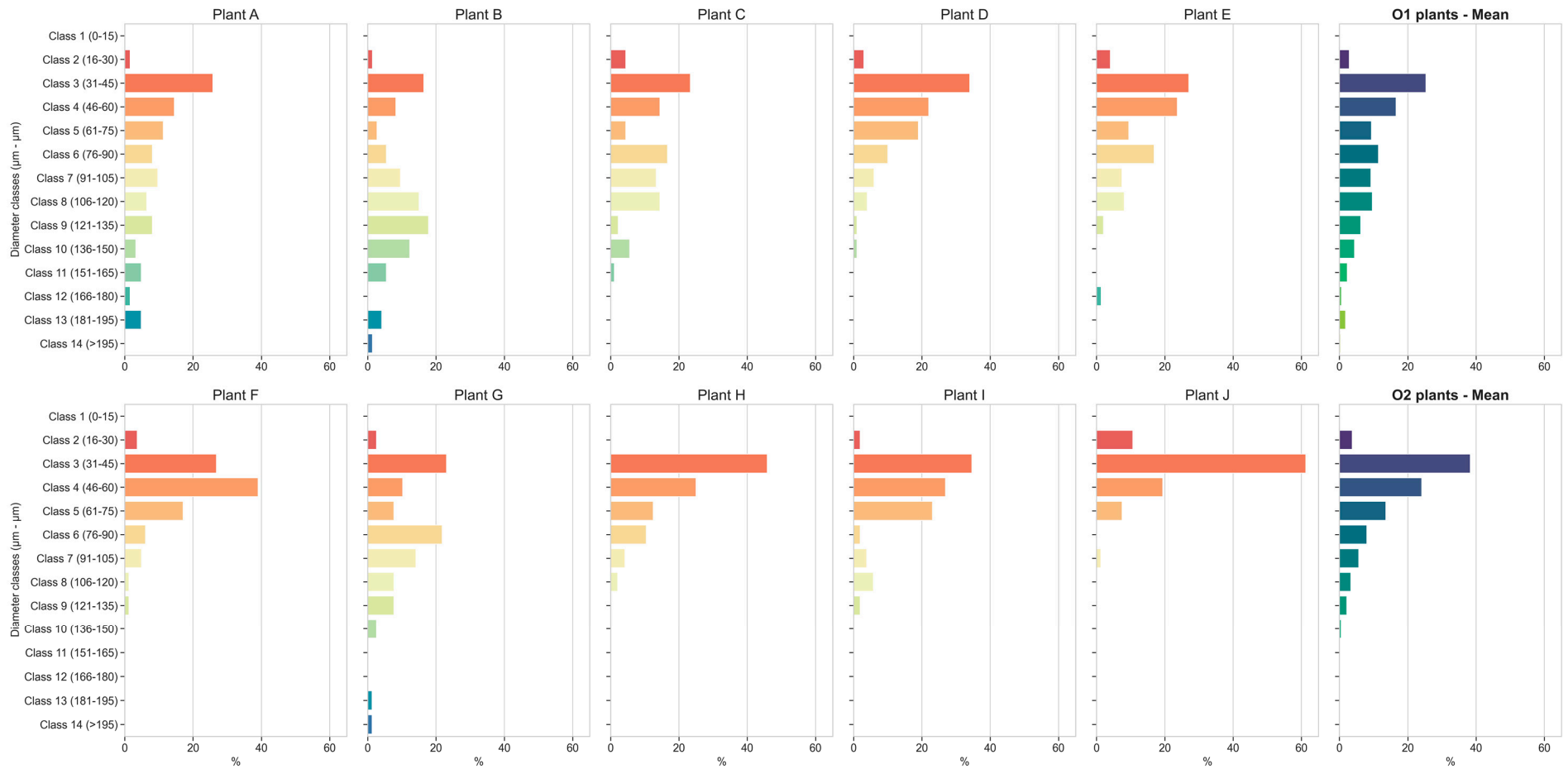


Figure 14. Distribution of xylem vessel diameter classes (µm): individual plants and mean values of five plants per orchard.

3.9. Root Xylem Vessel Density, Vessel Area and Vulnerability to Cavitation

The root xylem vessel density, vessel area and vulnerability to cavitation index (VI) detected in each plant and the mean values of five plants per orchard are reported in Table 4, where the final cumulative sap flow detected in 2022 is also reported. Plants from O2 evidenced a higher vessel density, with a 31.3 vessels mm^{-2} mean value, and individual values were always ≥ 24 vessels mm^{-2} . Plant J scored the highest vessel density (53.3 vessels mm^{-2}) and the lowest vessel area ($<700 \mu\text{m}^2 \text{mm}^{-2}$). Conversely, plants from O1 were characterised by a lower mean vessel density (25.2 vessels mm^{-2}), with the lowest value detected in plant A (15.5 vessels mm^{-2}), of which its vessel area was relatively high ($>3500 \mu\text{m}^2 \text{mm}^{-2}$), and the highest value detected was in plant E (37 vessels mm^{-2}). The mean vessel area of plants from O1 was more than double in comparison to plants from O2.

Table 4. Xylem vessel density, area and vulnerability index in roots sampled at the end of the vegetative season in 2022. The values of each plant and mean values of five plants per orchard are reported in parallel to the final cumulative sap flow.

		Vessel Density [n mm^{-2}]	Vessel Area [$\mu\text{m}^2 \text{mm}^{-2}$]	Vulnerability Index (VI) [$\mu\text{m mm}^{-2}$]	Cumulative Sap Flow [L]
O1	A	15.5	3777.05	5.45	90.66
	B	18.3	6022.54	5.90	119.52
	C	30.0	3749.98	2.57	188.64
	D	25.0	1757.91	2.77	171.72
	E	37.0	2509.74	1.79	204.68
	Mean value	25.2	3563.44	3.70	155.04
O2	F	27.3	1415.41	2.02	263.11
	G	26.0	3371.57	3.05	332.33
	H	24.0	1190.74	2.21	653.50
	I	26.0	1773.09	2.28	400.76
	J	53.3	685.06	0.82	543.14
	Mean value	31.3	1687.69	2.08	438.7

VI values were lower for plants from O2, with a mean value of 2.08 $\mu\text{m mm}^{-2}$; the highest VI was detected in plant G (3.05 $\mu\text{m mm}^{-2}$), while plant J scored the lowest value (0.82 $\mu\text{m mm}^{-2}$). Within the O1, the mean VI value was 3.7 $\mu\text{m mm}^{-2}$; two plants (A and B) showed very high VIs ($>5 \mu\text{m mm}^{-2}$), while plant E showed the lowest value (1.79 $\mu\text{m mm}^{-2}$); the VI value of plant E was also lower than most of those of plants from O2.

4. Discussion

Kiwifruit is a woody liana, with very long flexible vines and shallow fleshy roots. Xylem vessels are large to allow high rates of water conductance; in cultivated *Actinidia* spp., the xylem vessel diameters in younger stems are up to 80 μm [33], but larger diameters (up to 500 μm) are signalled in secondary xylem [69], and root xylem vessel diameters range from 120 to 500 μm [70]. For these reasons, kiwifruit is potentially highly vulnerable to water transport failure under drought stress.

In our survey, water availability was always optimal; however, the plants in O1 evidenced a water stress status, confirmed through the SWP, stomatal conductance and transpiration, which were significantly lower than those in O2: indeed, SWP, stomatal conductance and transpiration are considered the most precise indicators of the water status in plants. Moreover, the water volumes required for irrigation throughout the vegetative season were lower in O1, indicating a generally lower water uptake from the soil. As expected, due to the lower transpiration, a significantly higher leaf temperature was also detected in plants from O1 throughout the whole vegetative season; indeed, transpiration regulates the homeostasis of leaf temperature, and when transpiration is reduced due to low water availability or other stress factors inducing stomata closure, the leaf temperature can increase to harmful levels. Photosynthetic activity is directly hindered by high temperatures as well as by drought stress [70,71]; this could have contributed to the early growth arrest observed in plants from O1. Moreover, CO_2 assimilation rose with the increases in the stomatal conductance in all plants, whereas transpiration for the same

stomatal conductance was lower in plants from O1 when compared to plants from O2. This suggests that the reduced water flow from roots to leaves was not mainly caused by low stomatal conductance, but by xylem dysfunction. This hypothesis is also supported by the fact that no significant correlation was found between stomatal conductance and sap flow rate when measured simultaneously (correlation coefficients: -0.50 and -0.53 in O2 and O1, respectively). So, the volume of water flow through the xylem vessels seems not to be driven only by stomatal opening. Then, these data evidence that an impediment to the water flow through the xylem vessels was mostly present in plants from O1, so it can be inferred that the water stress status in these plants was due to impaired xylem functionality.

Water transport through xylem is mediated by negative pressure due to the water potential gradient between leaves and roots; when this gradient is high, water tension can become critical within the xylem vessel lumen causing cavitation or implosion, which greatly affect xylem hydraulic transport [35,72–74]. Under drought stress or when subjected to strong evaporative demand, plants can adopt different strategies of adaptation in order to limit the risk of impaired hydraulic conductance. Among these long-term strategies, plants can reduce sensitivity to cavitation by reducing the xylem vessel diameter. Decreased root xylem vessel diameters were observed in KiDS-affected plants, and this was proposed to be the result of a progressive adaptation to climate change, particularly to an increasing vapor pressure deficit [19,20]. Narrow xylem vessels provide safety from cavitation; nevertheless, a reduced xylem hydraulic conductance can also result, as well as a consequently reduced growth rate under favourable conditions [75]. A different strategy of adaptation to drought stress is the thickening of xylem vessel walls to withstand collapse. This implies a higher xylem construction cost; then, when photosynthetic efficiency is impaired, i.e., by high temperatures or by stomatal closure, the ability of the plant to defend itself from implosion can be hindered.

In our study, the sap flow monitored throughout two years showed a very significant difference among the two plant groups: both the cumulative sap flow and hourly sap flow rates were significantly higher in plants from O2 than from O1, suggesting an affected hydraulic conductance in the latter, particularly in 2022, which was a very hot and dry year. Plants from O1 showed a progressive decrease in the daily maximum flow rate starting from mid-June 2021, becoming less than half in comparison to the plants from the O2 during summer, and without recovery in autumn or in the following year. In O2, the maximum daily flow rate appeared with the highest frequency in the middle of the day during the whole two-year period, whereas in O1, the flow rate did not show a specific maximum peak during the day in the first year, while it showed a maximum early in the morning in the second year. Indeed, from September 2021, when the flow rate was already strongly lowered in plants from O1, and during the whole 2022, a peak of high flow rate began to appear early in the morning, approximately one hour after sunrise, followed by a sharp drop. This behaviour could be considered a sign of an emerging recovery of the flow after the night break, immediately stopped by an interruption of the flow through the xylem, that could be ascribed to xylem vessel hydraulic failure induced by sudden negative pressure occurring at the stomata opening.

In order to focus on the possible cause of the hydraulic failure, the root xylem vessel diameters were analysed. Interestingly, the more represented frequency classes of the distribution of xylem vessel diameters were between 30 and 45 μm ; then, in all plants, the xylem vessels were considerably narrower in comparison to the usual values reported in the literature, in the range of 120–500 μm [70]. This could be considered a general sign of the long-term adaptation to climate change of kiwifruit plants in this area, where a progressively rising VPD has been detected, as narrow vessels are less exposed to cavitation risk [19,20]. A broader distribution toward wider diameters was observed in plants from O1, indicating a lower adaptive ability and higher exposure to the risk of cavitation.

Moreover, the root xylem vessel density and area and the vulnerability to cavitation index were checked, and these parameters were examined in parallel with the cumulative sap flow. From the comparison between the two orchards, it emerged that plants from O1

are characterised by a higher vulnerability index, higher vessel area and lower vessel density than those of plants from O2, but with mean value differences not statistically significant; however, interesting information was also deduced by examining the characteristics of each plant. In plants from O1, the cumulated sap flow indicatively rose with increases in vessel density and with decreases in the vulnerability index; in particular, plants A and B are characterised by significantly higher vulnerability indexes, high vessel areas and low vessel densities, and significantly lower cumulated sap flows. Then, it could be speculated that both cavitation and a reduced xylem vessel number in roots may have contributed to the hydraulic failure of the whole plant, reducing the sap flow in the trunk, stem water potential and stomatal conductance and transpiration in leaf. However, plant E showed a very low VI (also lower than those of plants from O2) high vessel number, and its cumulative sap flow was the highest among plants from O1, but lower than those of all plants from O2. Moreover, the behaviours of plants from O2 were different, and no clear relation could be observed between the sap flow, vessel density and area and VI. So, it can be deduced that other factors, as well as cavitation and vessel density, could have affected the efficiency of the xylem water transport.

A possible hint could arise from the results of the dendrometric monitoring. This measurement allows us to check the growth trend and the water status of a plant at once: indeed, stem diameter changes consist of an irreversible component, due to growth, and a variable component, due to moisture content, that show a diurnal cycle. Diurnal diameter changes provide information about the sap flow and the water tension within the stem [44,45,68,76,77]. Under negative pressure within xylem vessels, the stem shrinks proportionally to the evaporative demand and to the wood density and elasticity. In our study, the dendrometric analysis revealed an early seasonal growth arrest and significantly higher daily stem diameter variations (SDVs) in plants from O1 compared to those from O2. The two orchards were very close, so the evaporative demand was presumably the same; then, the higher SDVs could indicate a higher elasticity of the wood of plants from O1, probably due to thinner vessel walls and lower lignification. The weak vessel walls, as well as the early seasonal growth arrest, can result from scarce photosynthetic efficiency, due to a low stomatal conductance, high leaf temperature and low SWP. Scarce photosynthetic efficiency hinders carbon storage to the detriment of root growth and turnover, xylogenesis, the refilling of embolised vessels, xylem vessel wall thickness, wood density and starch accumulation. The lack of thick xylem vessel walls makes the plant more vulnerable to implosion, which decreases sap flow by decreasing the vessel lumen diameter [35,40]; moreover, implosion can also trigger cavitation. Implosion and cavitation can also explain leaf petiole wilt, which appears as one of the earliest KiDS symptoms causing leaves to tilt downward, which sometimes anticipates leaf wilting.

Cavitation can also be responsible for stomatal closure [35,78]; so, the lower stomatal conductance detected since early morning in plants from O1 could be the consequence of cavitation occurring early in the day, soon after sunrise. This is also confirmed by overlapping the daily dynamics of sap flow rate and stem diameter, which revealed a very unusual behaviour in plants from O1: shrinkage was very marked even if the sap flow rate was very poor, and the maximum sap flow rate was detected early in the morning, corresponding exactly to the maximum stem diameter. This behaviour is unusual with respect to the model proposed by Herzog et al. [68], in which the daily maximum sap flow rate follows a declining phase of the stem radius. Indeed, during the night, the stem diameter usually increases, as stem rehydration takes place due to water storage replenishment, driven by a changing water potential in the absence of sap flow with an exchange of water between the xylem and phloem and related tissues (mainly cambium and parenchyma cells). In the morning, the sap flow increases after the sun reaches its maximum, usually in the middle of the day, corresponding to the stem shrinking phase; the minimum stem diameter is instead normally reached just before sunset, when the sap flow rate is in a decreasing phase. This behaviour was observed for plants from O2, but not for plants from O1, which were unable to both prevent cavitation and refill cavitated vessels.

Moreover, toward the end of the vegetative season, in plants from O1, the maximum daily shrinkage showed a reduction; this could be explained by a progressive depletion of plant water storage due to the lack of sufficient water uptake from the soil, and it is an index of a very serious water stress status [44]. Then, the arrest of growth can be explained concurrently by scarce photosynthetic activity and by inefficient hydraulic conductance, which cause scarce water and nutrient uptake even if available in the soil.

Therefore, the broader distribution toward wider diameters of root xylem vessels, their higher vulnerability to cavitation, the higher daily stem diameter variation and the higher stem vulnerability to implosion that characterise the anatomical features of O1 plants in comparison to O2 plants can explain the lower trunk sap flow; consequently, the lower stomatal conductance, transpiration and SWP can be explained by the lower amount of water that is delivered to the leaves, and the plants show symptoms of drought stress, even if water in the soil was assured through irrigation. A lower transpiration can explain higher leaf temperatures, due to the loss of homeostasis. High leaf temperatures and a low stomatal conductance can cause lower photosynthetic activity, thereby explaining the lower growth and lower resistance to implosion.

The interaction of cavitation, implosion and low vessel density could determine the conditions for KiDS symptom onset. This means that both short- and long-term responses to climate stress expose plants to the risk of KiDS development.

The different behaviours of plants from O1 and O2 could be due to a different timing of responses to climate stress, and the different timings could be due to other weakening factors, which can be searched for among the differences between the two orchards. The main differences were as follows: (i) the propagation material (cuttings and micropropagation through meristem culture in O2 and O1, respectively), (ii) soil preparation (ridged and flat soil in O2 and O1, respectively) and (iii) previous crop (grass and peach in O2 and O1, respectively). Other differences were also observed in the soil: (i) organic matter, CEC, the Ca/K ratio, assimilable iron (higher in O2) and (ii) phosphorus (higher in O1). In a previous survey carried out in 2022 on 125 Italian kiwifruit orchards [62], seven parameters were identified as significantly related to KiDS occurrence: (i) the propagation material (from micropropagation), (ii) the age of the propagation material (one year), (iii) the presence of PSA (*Pseudomonas syringae* pv *actinidiae*), (iv) the previous crop (tree crop), (v) the soil CEC (low), (vi) the soil salinity (low) and (vii) the soil chalk (low). In the present study, some of these results were confirmed: (i) the propagation material, (ii) the previous crop and (iii) the soil CEC.

Very interesting inputs come from the roles of the propagation material and previous crop. KiDS occurrence is related to the propagation material produced through micropropagation. Plants from cuttings develop larger root systems than plants grown through micropropagation, as observed by several farmers during the uprooting of adult plants (personal communications); however, micropropagation is widely diffused since the occurrence of PSA, as it ensures the absence of bacteria in the propagation material to prevent the spread of the infection. Nevertheless, the sterility of the propagation material also implies the removal of the natural microbioma of the plant; as a consequence, the beneficial effects of endophytes are lost, and new plants are more susceptible to the attack of pathogens [13,79]. This could explain why KiDS was found to also be related to PSA attacks [26] as well as to opportunistic microorganisms [14,80].

The importance of microbioma arises also from the role of previous crop: when kiwifruit is preceded by a tree crop, KiDS occurrence is more probable than when it is preceded by grass [26]. The positive effect of grass is probably due to the soil's residual biodiversity and biological fertility; when kiwifruit is preceded by a tree crop, beneficial microorganisms are lost, giving rise to a progressive deterioration of physical and biological soil properties, and leaving a negative legacy that lasts through time [13]. The preservation of natural soil biodiversity can play a significant role in root development and functionality [13], whereas the soil organic matter content is not implied in that, as it is not related to KiDS occurrence [26], as also confirmed by results previously obtained in

experimental orchards [19,20]. Moreover, the addition of selected useful microorganisms to soil, as well as soil ridging, which improves root aeration and avoids soil warming, can have a positive effect on the plant growth and physiological status, but can only delay KiDS onset [19,20]. Then, improper agronomic practices that do not respect the natural soil and plant equilibria, associated with climate change, in the long term can cause irretrievable damages.

Therefore, a paradigm shift should be undertaken when looking for effective agronomic management strategies aimed at preventing KiDS onset, giving more consideration to the peculiar plant physiology and needs within the changing environment. The roles of other KiDS predisposing factors, which until now, were not receiving enough attention, should be investigated more in depth.

5. Conclusions

A survey, carried out in a region strongly affected by kiwifruit decline syndrome and characterised by a rising temperature and vapor pressure deficit in recent decades, was conducted on healthy kiwifruit plants cv. Hayward. A strong narrowing of root xylem vessels was detected in all plants, which is considered an indicator of a long-term strategy of adaptation to changing climate. In some of the monitored plants, hydraulic conductance was affected by cavitation and implosion, which are indicative of short-term stress responses; this behaviour was detected when other predisposing factors were present in the orchard: previous tree crop and the propagation material from the meristem culture. These findings indicate that climate change should also be considered among the possible factors predisposing kiwifruit plants to KiDS, possibly because the plant weakness induced by impaired hydraulic conductance can make it more sensitive to other biotic or abiotic adversities, accelerating the onset and worsening of this syndrome's symptoms. Further investigations carried out under controlled conditions could allow us to better describe the stress response and the adaptative behaviour to a rising vapor pressure deficit in kiwifruit plants and possible interactions with other biotic and abiotic stress factors. The carbon balance should also be studied under rising temperatures, taking into account the needs for root growth and xylem vessel wall thickening.

Under productive conditions, the real water requirements of kiwifruit plants should be detected based on the indicators of the plant water status, such as a dendrometric detection of the daily stem diameter variation, instead of the soil water content, which fails to account for the water uptake and translocation capability of the plant; the daily stem diameter variation could also be adopted as an early indicator of possible KiDS onset before the symptoms appear. New agronomic management strategies should be undertaken, aimed at preventing KiDS onset, with more attention on plant and soil microbial biodiversity and on orchard microclimate control. Localised irrigation should be abandoned in favour of other systems that favour increasing the relative air humidity, thereby reducing the vapor pressure deficit, and that moisten a larger soil surface, which favours wider root development and better soil biodiversity preservation.

Author Contributions: Conceptualisation, L.B., C.M. (Chiara Morone) and L.N.; methodology, L.N., C.M. (Chiara Morone), L.B., S.M. and C.M. (Claudio Mandalà); software, F.P.; validation, C.M. (Claudio Mandalà) and L.B.; formal analysis, C.M. (Claudio Mandalà), S.M., F.P., G.F.B. and L.B.; investigation, C.M. (Claudio Mandalà), F.P. and G.F.B.; data curation, F.P.; writing—original draft preparation, C.M. (Claudio Mandalà) and L.B.; writing—review and editing, L.B.; visualisation, C.M. (Claudio Mandalà) and F.P.; supervision, L.B.; project administration, L.B.; funding acquisition, L.N. All authors have read and agreed to the published version of the manuscript.

Funding: This research was funded by Regione Piemonte, Direzione Agricoltura e Cibo, Settore Servizi di Sviluppo e Controlli per l'Agricoltura, Programma di ricerca, sperimentazione e dimostrazione agricola, Determinazione n. 432/A1706B del 21/05/2021 e Determinazione n. 1015/A1706B del 26/11/2021: Progetto "KIRIS-Approfondimento sull'eziologia e strumenti di prevenzione e difesa"-CUP n. J65C20000060007.

Data Availability Statement: Data are contained within the article.

Acknowledgments: The authors acknowledge and remember with great esteem and respect Barale and Vassallo for providing their own orchards for experimentation and for managing them with great accuracy and reliability; Marta Vallino (CNR-IPSP), Piermario Chiarabaglio and Simone Cantamessa (CREA FL) for their kindness and readiness to help with their skills and instruments for sample preparations for LM analysis; and Giovanna Cressano for flawless administrative support and for her willingness and helpfulness.

Conflicts of Interest: The authors declare no conflicts of interest.

References

1. FAO. FAOSTAT—Food and Agriculture Organization of the United Nations. Rome, Italy. Available online: <https://www.fao.org/faostat/en/#home> (accessed on 10 November 2023).
2. Scortichini, M.; Marcelletti, S.; Ferrante, P.; Petriccione, M.; Firrao, G. Pseudomonas Syringae Pv. Actinidiae: A Re-Emerging, Multi-Faceted, Pandemic Pathogen. *Mol. Plant Pathol.* **2012**, *13*, 631–640. [CrossRef]
3. Haye, T.; Weber, D.C. Special Issue on the Brown Marmorated Stink Bug, Halyomorpha Halys: An Emerging Pest of Global Concern. *J. Pest Sci.* **2017**, *90*, 987–988. [CrossRef]
4. Tacconi, G.; Tosi, L.; Giacomini, A.; Nari, L.; Berra, L.; Spadaro, D.; Prencipe, S.; Rosati, M.; Savian, F.; Saro, S.; et al. La Moria Del Kiwi al 2020: Lungi Dalla Soluzione! *Kiwi Inf.* **2020**, *16*, 6–16.
5. Savian, F.; Marroni, F.; Ermacora, P.; Firrao, G.; Martini, M. A Metabarcoding Approach to Investigate Fungal and Oomycete Communities Associated with Kiwifruit Vine Decline Syndrome in Italy. *Phytobiomes J.* **2022**, *6*, 290–304. [CrossRef]
6. Donati, I.; Cellini, A.; Sangiorgio, D.; Caldera, E.; Sorrenti, G.; Spinelli, F. Pathogens Associated to Kiwifruit Vine Decline in Italy. *Agriculture* **2020**, *10*, 119. [CrossRef]
7. Savian, F.; Martini, M.; Ermacora, P.; Paulus, S.; Mahlein, A.-K. Prediction of the Kiwifruit Decline Syndrome in Diseased Orchards by Remote Sensing. *Remote Sens.* **2020**, *12*, 2194. [CrossRef]
8. Tosi, L.; Tacconi, G.; Giacomini, A. La Moria Del Kiwi, Situazione e Prospettive. *L'informatore Agrar.* **2015**, *44*, 67–70.
9. Sorrenti, G.; Toselli, M.; Reggiori, G.; Spinelli, F. Implicazioni della gestione idrica nella “moria del kiwi” del veronese. *Riv. Fruttic. Ortofloric.* **2016**, *78*, 45–51.
10. Tacconi, G.; Paltrinieri, S.; Mejia, J.F.; Fuentealba, S.P.; Bertaccini, A.; Tosi, L.; Giacomini, A.; Mazzucchi, U.; Favaron, F.; Sella, L.; et al. Vine Decline in Kiwifruit: Climate Change and Effect on Waterlogging and Phytophthora in North Italy. *Acta Hort.* **2015**, *1096*, 93–97. [CrossRef]
11. Tacconi, G.; Giacomini, A.; Vittone, G.; Nari, L.; Spadaro, D.; Savian, F.; Ermacora, P.; Saro, S.; Morone, C.; Bardi, L.; et al. Il Punto Sulla Moria Del Kiwi a 8 Anni Dalla Sua Comparsa. *L'informatore Agrar.* **2019**, *75*, 34–36.
12. Bardi, L. Early Kiwifruit Decline: A Soil-Borne Disease Syndrome or a Climate Change Effect on Plant–Soil Relations? *Front. Agron.* **2020**, *2*, 3. [CrossRef]
13. Manici, L.M.; Saccà, M.L.; Scotti, C.; Caputo, F. Quantitative Reduction of Soil Bacteria and Qualitative Microbial Changes: Biotic Components Associated to Kiwifruit Decline. *Plant Soil* **2022**, *477*, 613–628. [CrossRef]
14. Spigaglia, P.; Barbanti, F.; Marocchi, F.; Mastroleo, M.; Baretta, M.; Ferrante, P.; Caboni, E.; Lucioli, S.; Scortichini, M. *Clostridium bifermentans* and *C. subterminale* Are Associated with Kiwifruit Vine Decline, Known as *moria*, in Italy. *Plant Pathol.* **2020**, *69*, 765–774. [CrossRef]
15. Prencipe, S.; Schiavon, G.; Rosati, M.; Nari, L.; Schena, L.; Spadaro, D. Characterization of Phytophthora Species Involved in the Establishment and Development of Kiwifruit Vine Decline Syndrome. *Microorganisms* **2023**, *11*, 216. [CrossRef]
16. Di Biase, R.; Calabritto, M.; Sofo, A.; Reyes, F.; Mininni, A.N.; Mastroleo, M.; Xylogiannis, E.; Dichio, B. Assessment of Kiwifruit Physiological Decline: Irrigation and Soil Management Strategy to Recover from Waterlogging. *Acta Hort.* **2023**, *1373*, 11–18. [CrossRef]
17. D'Ippolito, I.; Mang, S.M.; Elshafie, H.S.; Camele, I.; Scillitani, G.; Mastrodonato, M.; Sofo, A.; Mininni, A.N.; Xylogiannis, E. Morpho-Anatomical and Microbiological Analysis of Kiwifruit Roots with KVDS Symptoms. *Acta Hort.* **2022**, *1332*, 131–136. [CrossRef]
18. Sofo, A.; Mininni, A.N.; Dichio, B.; Mastroleo, M.; Xylogiannis, E. Physical Structure and Chemical Quality of Waterlogged Soils in an Italian Kiwifruit Orchard. *Acta Hort.* **2022**, *1332*, 195–202. [CrossRef]
19. Bardi, L.; Nari, L.; Morone, C.; Faga, M.G.; Malusà, E. Possible Role of High Temperature and Soil Biological Fertility on Kiwifruit Early Decline Syndrome. *Front. Agron.* **2020**, *2*, 580659. [CrossRef]
20. Bardi, L.; Nari, L.; Morone, C.; Solomita, M.; Mandalà, C.; Faga, M.G.; Migliori, C.A. Kiwifruit Adaptation to Rising Vapor Pressure Deficit Increases the Risk of Kiwifruit Decline Syndrome Occurrence. *Horticulturae* **2022**, *8*, 906. [CrossRef]
21. Reid, J.B.; Tate, K.G.; Brown, N.S.; Cheah, L.H. Effects of Flooding and Alluvium Deposition on Kiwifruit (*Actinidia deliciosa*): 1. Early Vine Decline. *N. Z. J. Crop Hortic. Sci.* **1991**, *19*, 247–257. [CrossRef]
22. Smith, G.S.; Judd, M.J.; Miller, S.A.; Buwalda, J.G. Recovery of Kiwifruit Vines from Transient Waterlogging of the Root System. *New Phytol.* **1990**, *115*, 325–333. [CrossRef] [PubMed]
23. Savé, R.; Serrano, L. Some Physiological and Growth Responses of Kiwi Fruit (*Actinidia chinensis*) to Flooding. *Physiol. Plant.* **1986**, *66*, 75–78. [CrossRef]

24. Smith, G.S.; Buwalda, J.G.; Green, T.G.A.; Clark, C.J. Effect of Oxygen Supply and Temperature at the Root on the Physiology of Kiwifruit Vines. *New Phytol.* **1989**, *113*, 431–437. [[CrossRef](#)]
25. Reid, J.B.; Tate, K.G.; Brown, N.S. Effects of Flooding and Alluvium Deposition on Kiwifruit (*Actinidia deliciosa*): 2. Vine Performance the Following Season. *N. Z. J. Crop Hort. Sci.* **1992**, *20*, 283–288. [[CrossRef](#)]
26. Servizio Fitosanitario Nazionale. Ministro Dell’agricoltura. della Sovranità Alimentare e delle Foreste Relazione del Progetto “Consulenza Tecnica Relativa All’elaborazione Dati di Monitoraggio Sulla Moria del Kiwi”. 2022. Available online: https://www.protezionedellepiante.it/wp-content/uploads/2022/09/220927_report-indagine-2021_moria_def (accessed on 8 February 2024).
27. Khan, M.U.A.; Khan, M.A.; Abbasi, U.A.; Amin, M.; Kalsoom, T.; Basit, A.; Shahzad, B. Kiwi Plant Growth Monitoring with Soil and Climatic Conditions in the Semi-Arid Region of Pakistan. *Environ. Sci. Proc.* **2023**, *23*, 36. [[CrossRef](#)]
28. Kataoka, I.; Matsuoka, M.; Beppu, K.; Ohtani, M. High Temperature Tolerance of Sanuki Kiwicco[®] Kiwifruit Interspecific Hybrid *Actinidia Rufa* × *A. Chinensis* Var. *Chinensis*. *Acta Hort.* **2022**, *1332*, 23–30. [[CrossRef](#)]
29. Richardson, A.; Eyre, V.; Rebstock, R.; Popowski, E.; Nardoza, S. Factors Influencing Flower Development in Kiwifruit Vines. *Acta Hort.* **2022**, *1332*, 141–154. [[CrossRef](#)]
30. Vetharanim, I.; Van Den Dijssel, C.; Stanley, J.; Richardson, A.; Müller, K. Projecting Suitability of Kiwifruit by Chill Requirements for Different Locations in New Zealand under Climate Change. *Acta Hort.* **2022**, *1332*, 455–462. [[CrossRef](#)]
31. Grossiord, C.; Buckley, T.N.; Cernusak, L.A.; Novick, K.A.; Poulter, B.; Siegwolf, R.T.W.; Sperry, J.S.; McDowell, N.G. Plant Responses to Rising Vapor Pressure Deficit. *New Phytol.* **2020**, *226*, 1550–1566. [[CrossRef](#)] [[PubMed](#)]
32. Grossiord, C.; Sevanto, S.; Borrego, I.; Chan, A.M.; Collins, A.D.; Dickman, L.T.; Hudson, P.J.; McBranch, N.; Michaletz, S.T.; Pockman, W.T.; et al. Tree Water Dynamics in a Drying and Warming World. *Plant Cell Environ.* **2017**, *40*, 1861–1873. [[CrossRef](#)]
33. Ferguson, A.R. Kiwifruit: A Botanical Review. In *Horticultural Reviews*; John Wiley & Sons, Ltd.: Hoboken, NJ, USA, 1984; pp. 1–64. ISBN 978-1-118-06079-7.
34. Domec, J.-C.; Palmroth, S.; Ward, E.; Maier, C.A.; Thérézien, M.; Oren, R. Acclimation of Leaf Hydraulic Conductance and Stomatal Conductance of *Pinus taeda* (Loblolly Pine) to Long-Term Growth in Elevated CO₂ (Free-Air CO₂ Enrichment) and N-Fertilization. *Plant Cell Environ.* **2009**, *32*, 1500–1512. [[CrossRef](#)] [[PubMed](#)]
35. Jacobsen, A.L.; Ewers, F.W.; Pratt, R.B.; Paddock, W.A.; Davis, S.D. Do Xylem Fibers Affect Vessel Cavitation Resistance? *Plant Physiol.* **2005**, *139*, 546–556. [[CrossRef](#)] [[PubMed](#)]
36. Carlquist, S. Ecological Strategies of Xylem Evolution. In *Ecological Strategies of Xylem Evolution*; University of California Press: Berkeley, CA, USA, 1975; ISBN 978-0-520-32056-7.
37. Hacke, U.G.; Sperry, J.S. Functional and Ecological Xylem Anatomy. *Perspect. Plant Ecol. Evol. Syst.* **2001**, *4*, 97–115. [[CrossRef](#)]
38. Donaldson, L.A. Abnormal Lignin Distribution in Wood from Severely Drought Stressed *Pinus radiata* Trees. *IAWA J.* **2002**, *23*, 161–178. [[CrossRef](#)]
39. Cochard, H.; Froux, F.; Mayr, S.; Coutand, C. Xylem Wall Collapse in Water-Stressed Pine Needles. *Plant Physiol.* **2004**, *134*, 401–408. [[CrossRef](#)] [[PubMed](#)]
40. Brodribb, T.J.; Holbrook, N.M. Water Stress Deforms Tracheids Peripheral to the Leaf Vein of a Tropical Conifer. *Plant Physiol.* **2005**, *137*, 1139–1146. [[CrossRef](#)] [[PubMed](#)]
41. Sperry, J.S.; Nichols, K.L.; Sullivan, J.E.M.; Eastlack, S.E. Xylem Embolism in Ring-Porous, Diffuse-Porous, and Coniferous Trees of Northern Utah and Interior Alaska. *Ecology* **1994**, *75*, 1736–1752. [[CrossRef](#)]
42. Santiago, L.S.; Goldstein, G.; Meinzer, F.C.; Fisher, J.B.; Machado, K.; Woodruff, D.; Jones, T. Leaf Photosynthetic Traits Scale with Hydraulic Conductivity and Wood Density in Panamanian Forest Canopy Trees. *Oecologia* **2004**, *140*, 543–550. [[CrossRef](#)] [[PubMed](#)]
43. Vilagrosa, A.; Bellot, J.; Vallejo, V.R.; Gil-Pelegrín, E. Cavitation, Stomatal Conductance, and Leaf Dieback in Seedlings of Two Co-occurring Mediterranean Shrubs during an Intense Drought. *J. Exp. Bot.* **2003**, *54*, 2015–2024. [[CrossRef](#)]
44. Fernández, J.E.; Cuevas, M.V. Irrigation Scheduling from Stem Diameter Variations: A Review. *Agric. For. Meteorol.* **2010**, *150*, 135–151. [[CrossRef](#)]
45. Dietrich, L.; Zweifel, R.; Kahmen, A. Daily Stem Diameter Variations Can Predict the Canopy Water Status of Mature Temperate Trees. *Tree Physiol.* **2018**, *38*, 941–952. [[CrossRef](#)] [[PubMed](#)]
46. Bardi, L.; Mandalà, C.; Monaco, S.; Nari, L.; Morone, C.; Neri, D. Per Rilevare Gli Stress Nel Kiwi Il Monitoraggio è Essenziale. *L’informatore Agrar.* **2023**, *15*, 41–45.
47. Beck, H.E.; Zimmermann, N.E.; McVicar, T.R.; Vergopolan, N.; Berg, A.; Wood, E.F. Present and Future Köppen-Geiger Climate Classification Maps at 1-Km Resolution. *Sci. Data* **2018**, *5*, 180214. [[CrossRef](#)] [[PubMed](#)]
48. Kottek, M.; Grieser, J.; Beck, C.; Rudolf, B.; Rubel, F. World Map of the Köppen-Geiger Climate Classification Updated. *Meteorol. Z.* **2006**, *15*, 259–263. [[CrossRef](#)] [[PubMed](#)]
49. USDA. *Keys to Soil Taxonomy*, 11th ed.; United States Department of Agriculture, Natural Resources Conservation Service: Washington, DC, USA, 2010.
50. FAO/ISRIC/ISSS. *World Reference Base for Soil Resources*; FAO: Rome, Italy, 1998.
51. Deloire, A.; Pellegrino, A.; Rogiers, S. A Few Words on Grapevine Leaf Water Potential. *IVES Tech. Rev. Vine Wine* **2020**, 1–2. [[CrossRef](#)]
52. Scholander, P.F.; Bradstreet, E.D.; Hemmingsen, E.A.; Hammel, H.T. Sap Pressure in Vascular Plants. *Science* **1965**, *148*, 339–346. [[CrossRef](#)] [[PubMed](#)]

53. Schneider, C.A.; Rasband, W.S.; Eliceiri, K.W. NIH Image to ImageJ: 25 Years of Image Analysis. *Nat. Methods* **2012**, *9*, 671–675. [[CrossRef](#)]
54. Schindelin, J.; Arganda-Carreras, I.; Frise, E.; Kaynig, V.; Longair, M.; Pietzsch, T.; Preibisch, S.; Rueden, C.; Saalfeld, S.; Schmid, B.; et al. Fiji: An Open-Source Platform for Biological-Image Analysis. *Nat. Methods* **2012**, *9*, 676–682. [[CrossRef](#)] [[PubMed](#)]
55. Van Rossum, G.; Drake, F.L. *Python 3: Reference Manual*; SohoBooks: New York, NY, USA, 2009; ISBN 978-1-4414-1269-0.
56. Zack, G.W.; Rogers, W.E.; Latt, S.A. Automatic Measurement of Sister Chromatid Exchange Frequency. *J. Histochem. Cytochem.* **1977**, *25*, 741–753. [[CrossRef](#)] [[PubMed](#)]
57. Tajima, R.; Kato, Y. Comparison of Threshold Algorithms for Automatic Image Processing of Rice Roots Using Freeware ImageJ. *Field Crops Res.* **2011**, *121*, 460–463. [[CrossRef](#)]
58. Cox, E.P. A Method of Assigning Numerical and Percentage Values to the Degree of Roundness of Sand Grains. *J. Paleontol.* **1927**, *1*, 179–183.
59. Feret, L.R. *La Grosseur des Grains des Matières Pulvérisées*; Eidgen. Materialprüfungsanstalt a. d. Eidgen. Technischen Hochschule: Zürich, Switzerland, 1931.
60. Walton, W.H. Feret's Statistical Diameter as a Measure of Particle Size. *Nature* **1948**, *162*, 329–330. [[CrossRef](#)]
61. Lemaire, C.; Quilichini, Y.; Brunel-Michac, N.; Santini, J.; Berti, L.; Cartailleur, J.; Conchon, P.; Badel, É.; Herbette, S. Plasticity of the Xylem Vulnerability to Embolism in *Populus Tremula* × *Alba* Relies on Pit Quantity Properties Rather than on Pit Structure. *Tree Physiol.* **2021**, *41*, 1384–1399. [[CrossRef](#)] [[PubMed](#)]
62. Carlquist, S. Ecological Factors in Wood Evolution: A Floristic Approach. *Am. J. Bot.* **1977**, *64*, 887–896. [[CrossRef](#)]
63. Scholz, A.; Klepsch, M.; Karimi, Z.; Jansen, S. How to Quantify Conduits in Wood? *Front. Plant Sci.* **2013**, *4*, 56. [[CrossRef](#)] [[PubMed](#)]
64. Hammer, Ø.; Harper, D.A.T.; Ryan, P.D. PAST: Paleontological Statistics Software Package for Education and Data Analysis. *Palaeontol. Electron.* **2021**, *4*, 4.
65. ARPA Piemonte Regional Agency for Environmental Protection. Available online: <https://www.arpa.piemonte.it/> (accessed on 4 December 2023).
66. Offenthaler, I.; Hietz, P.; Richter, H. Wood Diameter Indicates Diurnal and Long-Term Patterns of Xylem Water Potential in Norway Spruce. *Trees* **2001**, *15*, 215–221. [[CrossRef](#)]
67. Sevanto, S.; Hölttä, T.; Markkanen, T.; Perämäki, M.; Nikinmaa, E.; Vesala, T. Relationships between Diurnal Xylem Diameter Variation and Environmental Factors in Scots Pine. *Boreal Environ. Res.* **2005**, *10*, 447.
68. Herzog, K.M.; Häslér, R.; Thum, R. Diurnal Changes in the Radius of a Subalpine Norway Spruce Stem: Their Relation to the Sap Flow and Their Use to Estimate Transpiration. *Trees* **1995**, *10*, 94–101. [[CrossRef](#)]
69. Condon, J.M. Aspects of Kiwifruit Stem Structure in Relation to Transport. *Acta Hort.* **1992**, *297*, 419–426. [[CrossRef](#)]
70. Gould, N.; Clearwater, M.J. Vine Canopy and Root Physiology. In *Kiwifruit*; CABI: Oxfordshire, UK, 2023; pp. 255–272. [[CrossRef](#)]
71. Richardson, A.C.; Marsh, K.B.; Boldingh, H.L.; Pickering, A.H.; Bulley, S.M.; Frearson, N.J.; Ferguson, A.R.; Thornber, S.E.; Bolitho, K.M.; Macrae, E.A. High Growing Temperatures Reduce Fruit Carbohydrate and Vitamin C in Kiwifruit. *Plant Cell Environ.* **2004**, *27*, 423–435. [[CrossRef](#)]
72. Davis, S.D.; Ewers, F.W.; Sperry, J.S.; Portwood, K.A.; Crocker, M.C.; Adams, G.C. Shoot Dieback during Prolonged Drought in *Ceanothus* (Rhamnaceae) Chaparral of California: A Possible Case of Hydraulic Failure. *Am. J. Bot.* **2002**, *89*, 820–828. [[CrossRef](#)] [[PubMed](#)]
73. Woodrum, C.L.; Ewers, F.W.; Telewski, F.W. Hydraulic, Biomechanical, and Anatomical Interactions of Xylem from Five Species of *Acer* (Aceraceae). *Am. J. Bot.* **2003**, *90*, 693–699. [[CrossRef](#)]
74. Yang, S.; Tyree, M.T. A Theoretical Model of Hydraulic Conductivity Recovery from Embolism with Comparison to Experimental Data on *Acer Saccharum*. *Plant Cell Environ.* **1992**, *15*, 633–643. [[CrossRef](#)]
75. Venturas, M.D.; Sperry, J.S.; Hacke, U.G. Plant Xylem Hydraulics: What We Understand, Current Research, and Future Challenges. *J. Integr. Plant Biol.* **2017**, *59*, 356–389. [[CrossRef](#)] [[PubMed](#)]
76. Zimmermann, M.H.; Milburn, J.A. Transport and Storage of Water. In *Physiological Plant Ecology II: Water Relations and Carbon Assimilation*; Lange, O.L., Nobel, P.S., Osmond, C.B., Ziegler, H., Eds.; Encyclopedia of Plant Physiology; Springer: Berlin/Heidelberg, Germany, 1982; pp. 135–151. ISBN 978-3-642-68150-9.
77. Tyree, M.; Zimmermann, M. *Xylem Structure and the Ascent of Sap*; Springer: Berlin/Heidelberg, Germany, 2002; ISBN 978-3-642-07768-5.
78. Pratt, R.B.; Ewers, F.W.; Lawson, M.C.; Jacobsen, A.L.; Brediger, M.M.; Davis, S.D. Mechanisms for Tolerating Freeze–Thaw Stress of Two Evergreen Chaparral Species: *Rhus ovata* and *Malosma laurina* (Anacardiaceae). *Am. J. Bot.* **2005**, *92*, 1102–1113. [[CrossRef](#)] [[PubMed](#)]
79. Anguita-Maeso, M.; Trapero-Casas, J.L.; Olivares-García, C.; Ruano-Rosa, D.; Palomo-Ríos, E.; Jiménez-Díaz, R.M.; Navas-Cortés, J.A.; Landa, B.B. Verticillium Dahliae Inoculation and in Vitro Propagation Modify the Xylem Microbiome and Disease Reaction to Verticillium Wilt in a Wild Olive Genotype. *Front. Plant Sci.* **2021**, *12*, 632689. [[CrossRef](#)] [[PubMed](#)]
80. Prencipe, S.; Savian, F.; Nari, L.; Ermacora, P.; Spadaro, D.; Martini, M. First Report of Phytophthora Vexans Causing Decline Syndrome of Actinidia Deliciosa ‘Hayward’ in Italy. *Plant Dis.* **2020**, *104*, 2032. [[CrossRef](#)]

Disclaimer/Publisher’s Note: The statements, opinions and data contained in all publications are solely those of the individual author(s) and contributor(s) and not of MDPI and/or the editor(s). MDPI and/or the editor(s) disclaim responsibility for any injury to people or property resulting from any ideas, methods, instructions or products referred to in the content.